**Journal of Information Systems Engineering and Management**
2025, 10(42s)
e-ISSN: 2468-4376
https://www.jisem-journal.com/

**Research Article**

# A Computational Neural Network Model Depicting Bradykinesia in Parkinson's Disease

Ms. Akanksha Kaushik[1*], Dr. Jyotsna Singh[2], Dr. Shilpa Mahajan[3]

[1*]*Computer Science and Engineering, School/College: School of Engineering and Technology (SOET), University: The North Cap University, City: Gurugram, State with ZIP/PIN: 122017, Country: India, Email: akanksha18csd002@ncuindia.edu*

[2]*Director I/C NMIMS Chandigarh and Associate Dean,STME, NMIMS Chandigarh, State with ZIP/PIN: 160014, Country: India, Email: singhjyotsna1@gmail.com*

[3]*Computer Science and Engineering, School/College: School of Engineering and Technology (SOET), University: The North Cap University City: Gurugram, State with ZIP/PIN: 122017, Country: India, Email: shilpa@ncuindia.edu*

**ARTICLE INFO**

Received: 24 Dec 2024

Revised: 12 Feb 2025

Accepted: 26 Feb 2025

**ABSTRACT**

Parkinson's disease (PD) is caused by a deficiency of dopamine (DA) as a result of cell death in the ventral tegmental area (VTA) and substantia nigra pars compacta (SNc). Though most computational studies of Parkinson's disease (PD) have concentrated on the effects of dopamine depletion in the basal ganglia, it's crucial to remember that the spinal cord, frontal and parietal cortex, and other areas have considerable dopamine innervation. A network model must be created to investigate how patterns of dopamine depletion across important cellular sites in the spinal cord, cortex, and basal ganglia affect the disruption of spinal cord and neuronal activity in addition to other PD symptoms in order to fully comprehend PD symptoms such as bradykinesia. We integrate dopaminergic innervation of cells in the cortical and spinal components of the basal ganglia-cortico-spinal circuit that governs voluntary arm motions. Many of the main impacts of DA depletion on neuronal, electromyographic (EMG), and movement parameters linked to Parkinson's disease (PD) bradykinesia are effectively replicated in the resultant model.

**Keyword**: Parkinson' disease; Dopamine; Bradykinesia; Cortex; Basal ganglia; Spinal cord

## INTRODUCTION

Parkinson's disease is a progressive neurodegenerative disorder which is pathologically characterized by the degeneration of dopamine in the substantia nigra of the basal ganglia. Bradykinesia stands as the quintessential and most debilitating symptom of Parkinson's disease (PD). In the early stages of the illness, its most prominent indication is the challenge in activities such as walking, speaking, or transitioning between seated and standing positions (Gibberd, 1986). Patients may exhibit a lack of arm swing during walking or a diminished facial expression (Abbs, Hartman, & Vishwanat, 1987; Gibberd, 1986; Weiner & Singer, 1989). As the disease progresses, bradykinesia begins to influence all movements and late on may lead to a comprehensive loss of mobility.

Patients find themselves needing strong focus to overcome the noticeable weakness in their limbs, even for the most basic motor tasks. Notably, initiating movement becomes notably challenging when attempting unfamiliar or unconventional actions (Connor & Abbs, 1991), or when coordinating multiple movements simultaneously (Benecke, Rothwell, & Dick, 1986; Lazarus & Stelmach, 1992).

The etiology of bradykinesia remains partly unclear due to the intricate network of pathways connecting sites of neuronal degeneration to muscle function. Key pathways include: (1) the route from the substantia nigra pars compacta (SNc) and ventral tegmental area (VTA) to the striatum, then to the substantia nigra pars reticulata (SNr) and the globus pallidus internal segment (GPi), onward to the thalamus and frontal cortex; (2) the pathway from the SNc/VTA to the striatum, SNr, and GPi, extending to the brainstem; and (3) the pathway from the SNc/VTA to cortical regions like the supplementary motor area (SMA), parietal cortex, and primary motor cortex (M1), then projecting to the spinal cord. These diverse pathways underscore the complexity of bradykinesia's neural circuitry and contribute to the challenge of pinpointing its precise origins.

Journal of Information Systems Engineering and Management
2025, 10(42s)
e-ISSN: 2468-4376
https://www.jisem-journal.com/

Research Article

The prevailing perspective suggests that cortical motor centre's suffer from insufficient activation due to excitatory circuits passing through the basal ganglia (BG) (Albin, Young, & Penney, 1989). Consequently, motor neuron pools receive inadequate facilitation, leading to diminutive and feeble movements (Albin et al., 1989). Implicit in this viewpoint is the assumption that cells in the cortex and spinal cord maintain normal functionality. However, this paper will propose an alternative interpretation.

This paper integrates experimental findings regarding the anatomy, neurophysiology, and neurochemistry of the globus pallidus internal segment, cortex, and spinal cord structures, alongside data on motor impairments in Parkinson's disease (PD). Our aim is to expand upon an established neural model of basal ganglia-cortex-spinal cord interactions during movement production (Bullock & Grossberg, 1988, 1989, 1991, 1992; Bullock & Contreras-Vidal, 1993; Contreras-Vidal, Grossberg, & Bullock, 1997; Bullock, Cisek, & Grossberg, 1998). Through computer simulations, we demonstrate that disruptions in basal ganglia output and dopamine input from the substantia nigra pars compacta (SNc) to the frontal and parietal cortices, as well as the spinal cord, may underlie delayed movement initiation.

The central hypothesis posits that the absence of dopamine modulation from the SNc disrupts, via multiple pathways, the establishment of movement-related response patterns in the primary motor and parietal cortex. This disruption results in a loss of directional specificity among reciprocal and bidirectional cells in the motor cortex, along with decreased activity levels and rates of change. Consequently, there are delays in recruiting the appropriate muscle force levels swiftly and in accurately scaling dynamic muscle force to movement parameters. In some cases, a repetitive triphasic pattern of muscle activation becomes necessary to complete the movement. Collectively, these alterations lead to prolonged mean reaction times and reduced movement speed, indicative of bradykinesia.

## LITERATURE REVIEW

### Dopaminergic Innervation in the Spinal Cord and Primate Neocortex

Recent research has unveiled the widespread presence of dopaminergic innervation in the primate neocortex and spinal cord (Bjorklund & Lindvall, 1984; Williams & Goldman-Rakic, 1998), implicating its involvement in various psychiatric and neurological disorders, including Parkinson's disease and schizophrenia. The dopaminergic fibers in the neocortex are believed to originate from neurons located in the substantia nigra (SN), the ventral tegmental area (VTA), and the retrorubral area (RRA) (Williams & Goldman-Rakic, 1995).

Dopaminergic afferents are most concentrated in the anterior cingulate (area 24) and motor areas (areas 4, 6, and SMA), exhibiting a tri-laminar distribution pattern primarily in layers I, IIIa, and V–VI (Berger et al., 1988; Elsworth et al., 1990; Gaspar et al., 1991; Gaspar et al., 1992; Williams & Goldman-Rakic, 1998). In granular prefrontal (areas 46, 9, 10, 11, 12), parietal (areas 1, 2, 3, 5, 7), temporal (areas 21, 22), and posterior cingulate (area 23) cortices, dopaminergic afferents are less dense, displaying a bilaminar distribution pattern primarily in layers I and V–VI (Gaspar et al., 1991, 1992; Lewis et al., 1988; Lidow et al., 1989; Berger et al., 1988). Notably, the lowest density of dopamine afferents is observed in area 17, where they are predominantly confined to layer I (Berger et al., 1988).

Multiple studies have documented the presence of dopaminergic fibers in the spinal cord, in addition to their innervation of the neocortex (Bjorklund & Skagerberg, 1979; Blessing & Chalmers, 1979; Takada, Li, & Hattori, 1988). These dopaminergic fibers are primarily concentrated in the superficial layers, laminae III–V of the dorsal horn, and lamina X. Originating from the posterior and dorsal hypothalamic areas, as well as the periventricular gray matter of the caudal thalamus, these fibers extend into the spinal cord.

Research suggests that dopaminergic fibers in the spinal cord may partly originate from neurons in the substantia nigra (Commissiong, Gentleman, & Neff, 1979). Unilateral lesions of the substantia nigra induced by 6-hydroxydopamine (6-OHDA) injection notably decrease dopamine levels in both the striatum and the spinal cord on the injected side. This finding implies the presence of an uncrossed nigrospinal dopaminergic pathway. However, anatomical methods have yet to confirm such direct input to the spinal cord.

Recent investigations suggest the presence of dopaminergic innervation in the ventral horn (layers VII and VIII, and lamina IX) as well (Weil-Fugazza & Godefroy, 1993). Dopamine receptors D1 and, to a lesser extent, D2, are distributed throughout both the dorsal and ventral spinal cord (Dubois, Savasta, Curet, & Scatton, 1986). The ventral

**Journal of Information Systems Engineering and Management**
2025, 10(42s)
e-ISSN: 2468-4376
https://www.jisem-journal.com/

**Research Article**

dopaminergic innervation originates from the caudal hypothalamus A11 cell group (Shirouzou, Anraku, Iwashita, & Yoshida, 1990). To understand the diverse dopaminergic systems and their connections to the cortex and spinal cord, we have referred the comprehensive review by Bjorklund & Lindvall (1984). Fig 1 presents a schematic diagram depicting the dopaminergic innervation of the basal ganglia (BG) and the sensory- motor cortex.

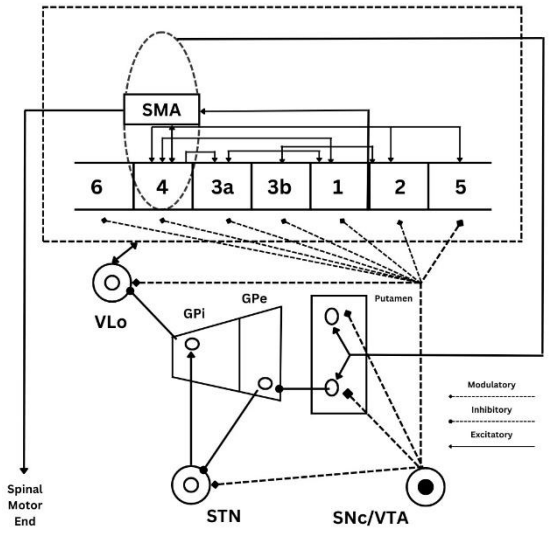


***Fig 1:*** *Diagram illustrating the dopaminergic innervation of the basal ganglia and sensory-motor cortex. Solid lines with arrow endings represent excitatory projections, while solid lines with dot endings denote inhibitory projections. Dotted lines with diamond endings indicate dopamine (DA) modulatory projections. Key structures include the subthalamic nucleus (STN), globus pallidus internal segment (GPi), globus pallidus external segment (GPe), ventrolateral thalamus (VLo), substantia nigra pars compacta (SNc), ventral tegmental area (VTA), and supplementary motor area (SMA). Cortical areas are labeled according to the Brodmann classification (1, 2, 3a, 3b, 4, 5, 6).*

The parameters for the normal functioning of the basal gangliocortico-spinal network are defined as: $G_o$=0.6, k=1, h=0.18, Im=1, l=0.95, T1=1.4, T2=0.3, $G_i$=0.9, Gv=2, Gs=1, $G_f$=1, g=1, b=15.5, and $DA_{1-8}$=1 (Bullock et al., 1998; Contreras-Vidal et al., 1997).

## Previous models

### Contreras-Vidal and Stelmach model

Contreras-Vidal & Stelmach (1995) introduced a comprehensive model outlining the intricate relations between the basal ganglia, thalamus, and cortex in both normal and parkinsonian movements (Contreras-Vidal, 1999). Central to the model's architecture was the incorporation of the 'direct' and 'indirect' pathways framework of the basal ganglia. Within this model, cortical input was shared by a pair of adjacent putamen output neurons.

Competitive interactions in the putamen, facilitated by feedback surround inhibition, served to enhance contrast and suppress noise in cortical inputs. Output projections from the putamen formed distinct parallel pathways (direct and indirect) to the globus pallidus internal segment (GPi). The direct pathway led to GPi cell inhibition, while the indirect pathway activated GPi neurons via the inhibitory route through the external segment of the globus pallidus (GPe) and the excitatory path through the subthalamic nucleus (STN). Acting as a normally closed gate, the GPi could be transiently opened by physically activating the direct pathway and closed by activating the indirect pathway. Opening the gate through GPi inhibition led to disinhibition of the motor thalamus (ventrolateral nucleus, VLo), thereby activating the same cortical areas that initiated striatal activation.

The model also incorporated an opponent neurochemical differentiation, reflecting the differential neurochemical and neurophysiological disturbances resulting from dopamine (DA) depletion. This included the presence of GABA, substance P (SP), and dynorphin (DYN) in the direct pathway, and GABA and enkephalin (ENK) in the indirect

**Journal of Information Systems Engineering and Management**
2025, 10(42s)
e-ISSN: 2468-4376
https://www.jisem-journal.com/

**Research Article**

pathway. Furthermore, the majority of striatal cells projecting to GPi expressed the D1 dopamine (DA) receptor, while those projecting to GPe mainly expressed the D2 DA receptor.

The model's predictions suggested that akinesia and bradykinesia in Parkinson's disease (PD) were not the result of malfunctioning independent basal ganglia processes. Instead, these features formed a continuum, ranging from normal reaction time (RT) and movement time (MT) to delayed RT and prolonged MT, culminating in akinesia.

### Brown, Bullock and Grossberg model

Brown, Bullock, and Grossberg (2004) introduced an extensive neural network model focused on saccadic eye movements across various experimental conditions, including fixation, saccade, overlap, gap, and delayed tasks. While the model aimed to meet the sequential requirements of conditional voluntary behavior by exploring the interactions between the basal ganglia (BG) and laminar circuits in the frontal cortex and superior colliculus, it also developed a detailed model of the BG.

According to this model, the contextual gating of reactive plans by basal ganglia structures plays a crucial role in plan execution, which is initiated by the activation of the direct pathway. Unlike other models proposed by Berns & Senjowski (1995), Contreras-Vidal (1999), and Taylor & Taylor (2000), competition for plan expression is facilitated by the activation of striatal GABAergic inhibitory interneurons rather than by recurrent inhibition of striatal excitatory neurons. Additionally, the model suggests that activation of the indirect pathway enables the deferral (STOP signal) of a selected plan, while the thalamo-striatal feedback signal guides the learning of deferral responses within the indirect pathway.

## METHODOLOGY USED

### Network Architecture

Figure 2 illustrates the components of the basal ganglio-corticospinal network model. For the basal ganglio-cortical network, we adopted the VITE (Vector Integration to End point) model proposed by Bullock & Grossberg (1988), which we have extended in this study. The original VITE model was selected because it (1) can generate single joint arm movements (Bullock & Grossberg, 1988), and (2) allows for the functional interpretation and simulation of properties observed in various types of identified cortical neurons (Bullock et al., 1998).

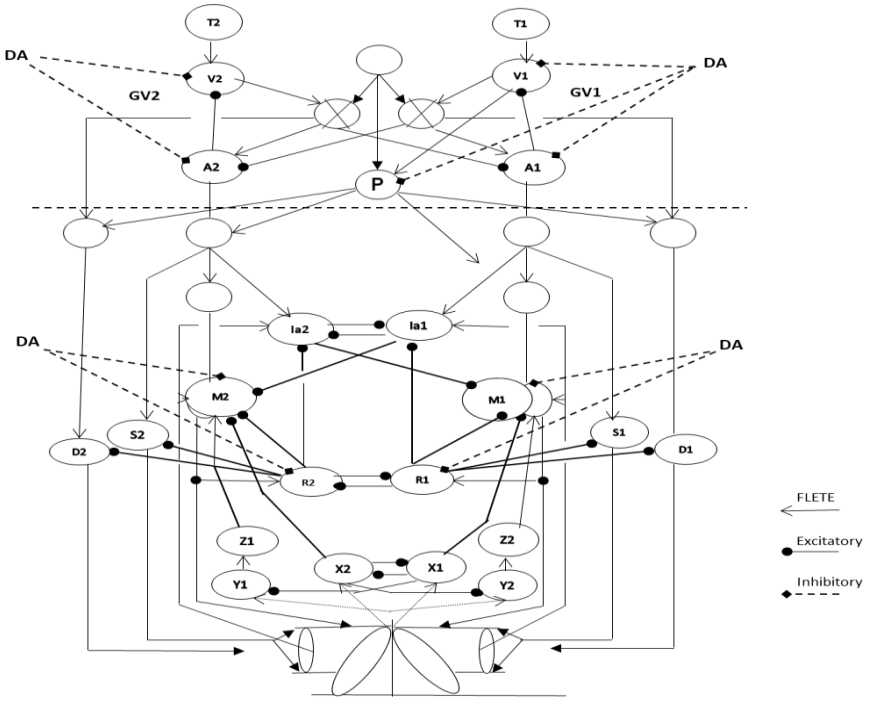


***Figure 2:*** *Network Architecture to show the components of the basal ganglio-corticospinal*

**Journal of Information Systems Engineering and Management**
2025, 10(42s)
e-ISSN: 2468-4376
https://www.jisem-journal.com/

**Research Article**

In our work, the VITE model is modified (Bullock & Grossberg, 1988, 1989, 1991, 1992) and extended the range of cortically identified neuron types and their properties, while also investigating the effects of dopamine depletion on key cortical cellular sites. Within the model, a difference vector (DV) for arm movement is computed in parietal area 5 by comparing a target position vector (TPV) with a representation of the current position known as the perceived position vector (PPV).

Subsequently, the DV signal is projected to area 4, where it interacts with a desired velocity vector (DVV) and a non-specific co-contractive signal (P) (Humphrey & Reed, 1983). A voluntarily scalable "GO" signal modulates (or "gates") the DV input to both the DVV and P in area 4, thereby generating velocity commands sensitive to volitional control and non-specific co-contractive commands. These commands then activate the lower spinal centers.

The DVV and P signals represent two partially independent neuronal systems within the motor cortex. DVV reflects the activity of reciprocal neurons, organized to facilitate the reciprocal activation of antagonist muscles (Doudet et al., 1990). On the other hand, P reflects the activity of bidirectional neurons, which adjust their activity for both movement directions (Doudet et al., 1990), and is organized to induce co-contraction of antagonist muscles.

While the reciprocal pattern of muscle activation drives joint movement from an initial to a final position, antagonist co-contraction enhances the mechanical stiffness of the joint, thereby stabilizing its posture or trajectory against external force perturbations (Bullock & Contreras-Vidal, 1993; Humphrey & Reed, 1983).

The spinal component of our modified VITE model commands corresponds to the FLETE (Factorization of Length and Tension) model (Bullock & Contreras-Vidal, 1993; Bullock & Grossberg, 1989, 1991, 1992). In essence, the FLETE model represents an opponent processing muscle control framework that elucidates how spinal circuits facilitate independent voluntary control of joint stiffness and position. Notably, it incorporates second-order dynamics, which significantly contribute to the realism of limb movements.

Our adaptation extends the original FLETE model by integrating the influence of the now cortically controlled co-contractive signal onto its spinal elements. In the original FLETE model, the co-contraction signal was merely a parameter, but in our variant, it is dynamically modulated by cortical inputs. Additionally, we investigate the impact of dopamine depletion on key spinal centers and its effects on voluntary movements.

## Mathematical Equations

It's important to note that the equations (1, 6, 7, 8–12, 14, 15, 17–31) presented in this section draw upon the work of several prior researchers (Bullock & Contreras-Vidal, 1993; Bullock & Grossberg, 1988, 1989, 1991, 1992; Bullock et al., 1998; Contreras-Vidal et al., 1997). While some equations (2, 5, 13, 16) have been modified to incorporate the effects of dopamine, we also introduce new equations (3 and 4). To enhance the clarity and accessibility of this section for readers, we provide a comprehensive list of all equations (both old and new) utilized in the model.

In the model, the output of the basal ganglia (BG) system, specifically the activity of the globus pallidus internal segment (GPi) (Horak & Anderson, 1984), is represented by the GO signal, where Go scales the GO signal.

$$G(t) = G_0(t - \varphi_i)^2 u[t - \varphi_i]/(\beta + \gamma(t - \varphi_i)^2 \quad (1)$$

Here, i denotes the onset time of the ith volitional command, while b and g are free parameters, and u[t] is a step function that transitions from 0 to 1 to initiate movement. The phasic cell activity in area 5 (Chapman, Spidalieri, & Lamarre, 1984; Kalaska, Cohen, Prud'Homme, & Hyde, 1990), which is depicted by the difference vector (DV), is described as follows:

$$\frac{dV_i}{dt} = 30(-V_i + T_i - DA_1 A_i) \quad (2)$$

Here, Ti represents the target position command, Ai denotes the current limb position command, and DA1 signifies the modulatory effect of dopamine on the inputs to area 40's perceived position vector (PPV) influencing DV cell activity. The values of dopamine can vary between 0 (lesioned) to 1 (normal) (see Figs. 3 and 4).

**Journal of Information Systems Engineering and Management**
2025, 10(42s)
e-ISSN: 2468-4376
https://www.jisem-journal.com/

**Research Article**

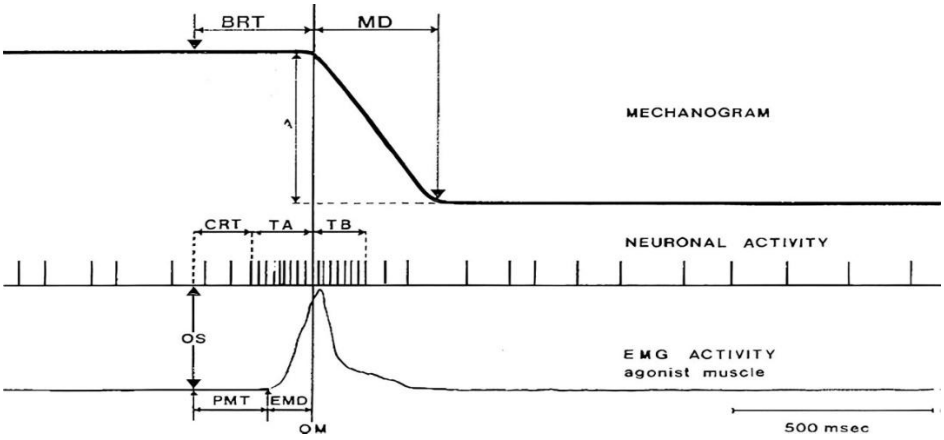


***Fig 3**: Illustration depicting the parameters under investigation. Movement parameters are depicted in the upper diagram, including behavioral reaction time (BRT in ms), movement duration (MD in ms), and movement amplitude (A in degrees). Neuronal activity parameters are shown in the middle diagram, featuring cellular reaction time (CRT in ms) and the duration (ms) of burst discharge preceding (Ta) and following (Tb) the onset of movement (OM), represented by the vertical line. EMG activity parameters are illustrated in the lower diagram, highlighting premotor time (PMT in ms) and electromechanical delay (EMD in ms).*

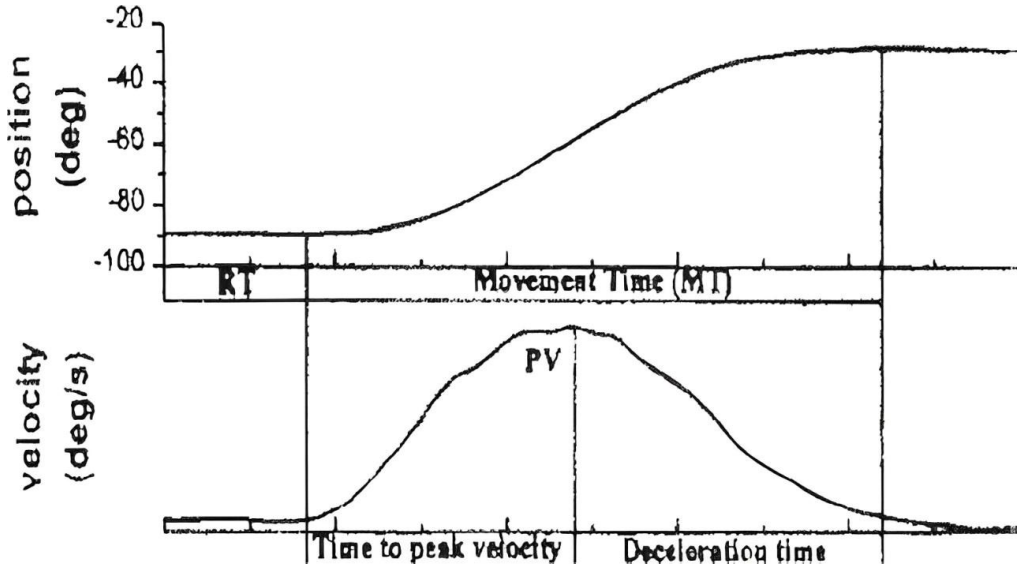


***Fig 4:** The position and velocity profiles of elbow movement from a typical young subject are illustrated. Various kinematic and temporal variables are indicated, including reaction time (RT), movement time (MT), peak velocity (PV), time-to-peak velocity (TPV), and deceleration time (DT).*

The desired velocity vector (DVV), which reflects the activity of reciprocally activated cells in area 4 (Doudet et al., 1990; Georgopoulos, Kalaska, Caminiti, & Massey, 1982; Kalaska, Cohen, Hyde, & Prud'Homme, 1989), is defined by:

$$u_i = \left[G\left(DA_2V_i - DA_3V_j\right) + \frac{Bu}{DA_4}\right]^+ \quad (3)$$

where i and j represent opponent neural commands, Bu denotes the baseline activity of the phasic-MT area 4 cell activity, and DA2 and DA3 signify the modulatory effects of dopamine on the inputs to DVV cell activity, while DA4 represents the effect of dopamine on the baseline activity of DVV. Notably, Eq. (3) illustrates that the DV flexion (Vi) cell is influenced by a distinct DA parameter (DA2) compared to the DV extension (Vj) cell (DA3).

Journal of Information Systems Engineering and Management
2025, 10(42s)
e-ISSN: 2468-4376
https://www.jisem-journal.com/

Research Article

As depicted in Table 1, under normal conditions, the values of DA2 and DA3 are equal to 1, whereas in the case of dopamine depletion, the value of DA2 is smaller than that of DA3. This model assumption is corroborated by experimental observations from studies conducted by Doudet et al. (1990) (see Figs. 5 and 6) and Watts & Mandir (1992) (column 1 of Fig. 7).

**Table 1: Summary of model's output neuronal, muscular, and movement parameters for normal and dopamine-depleted conditions**

| | | |
|---|---|---|
| **CRT** | 3.035 | 3.075 |
| **$T_A$** | 10.07 | 14.83 |
| **$T_B$** | 3.59 | 21.08 |
| **PMT** | 0.025 | 0.027 |
| **EMD** | 13.19 | 17.99 |
| **RT** | 13.25 | 18.05 |
| **MT** | 18.5 | 60.48 |
| **TPV** | 3.69 | 4.58 |
| **DT** | 14.9 | 55.98 |
| **Peak DVV** | 0.2 | 0.14 |
| **Peak EMG** | 1.4 | 1.12 |
| **Peak velocity** | 0.21 | 0.18 |
| **Force** | 0.065 | 0.045 |

Units: time (ms).

- Normal parameter set, $G_0$= 0.5, β = 100.3, ϒ = 0.71, $DA_{1–8}$= 1;
- Dopamine-depleted parameter set, $G_0$ = 0.15, β = 100.4, ϒ = 0.6, $DA_1$=0.79, $DA_2$=0.71,

$DA_3$=0.8, $DA_4$=0.8, $DA_5$=0.85, $DA_6$=0.7, $DA_7$= 0.75, $DA_8$=0.85

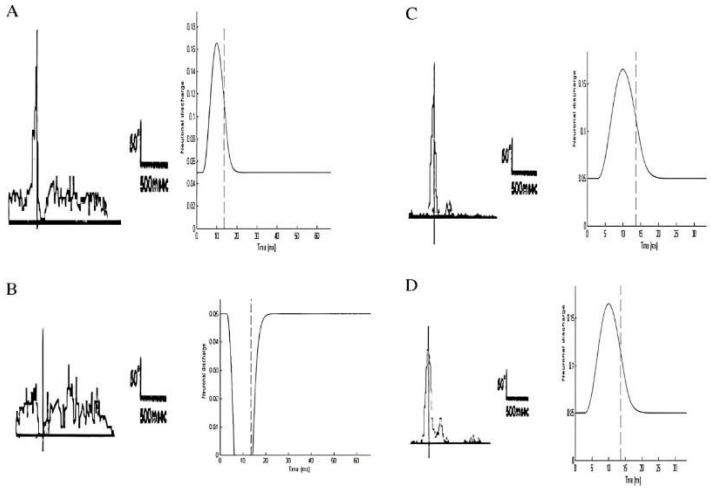


***Fig 5:*** *Comparison of changes in the peristimulus time histograms (PSTH) of area 4's reciprocally organized neurons in simulated area 4's reciprocally organized phasic (DVV) cell activities in PSTH of area 4's bidirectional neurons, and in simulated area 4's co-contractive (P) cell activities (column 4) for flexion (A and C) and extension (B and D) movements in a normal monkey. The vertical bars indicate the onset of movement. Spike discharges related to successive movements are accumulated into histograms, with each bin corresponding to 10 ms. In the simulations, a GO signal of G=0.6, b=0.5, g=0.8, and dopamine DA1–8=1 (normal) was used. Note that 1 s of time is approximately 100-time steps.*

**Journal of Information Systems Engineering and Management**
2025, 10(42s)
e-ISSN: 2468-4376
https://www.jisem-journal.com/

**Research Article**

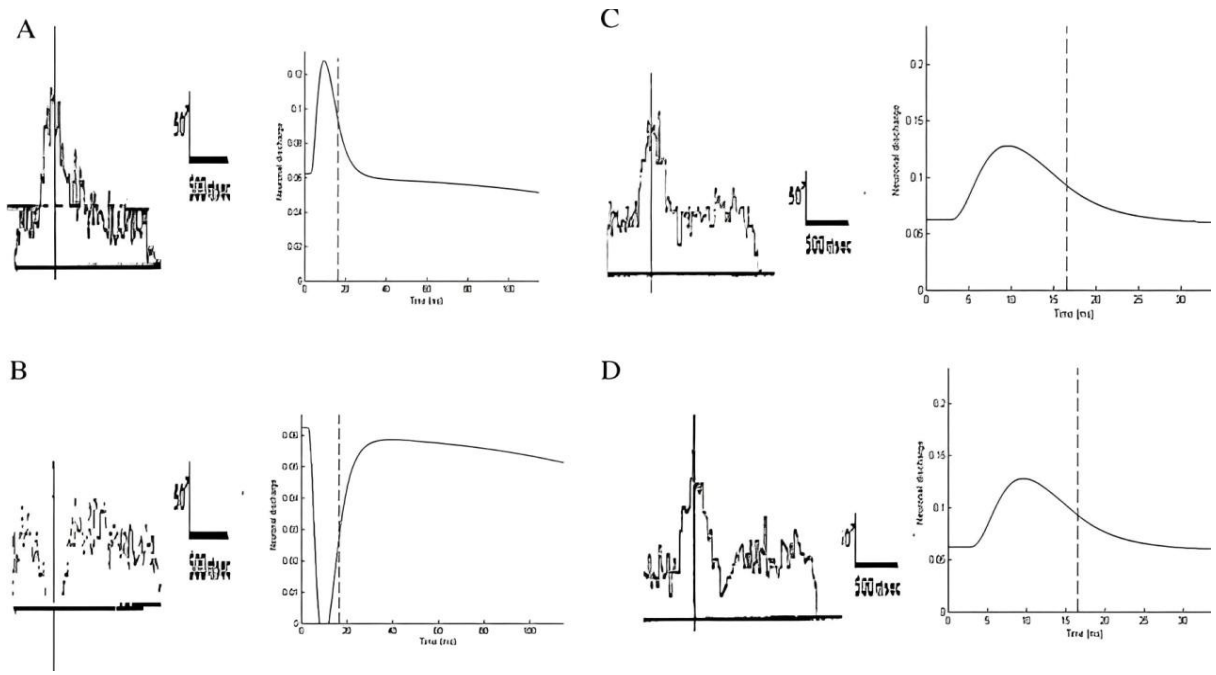


***Fig 6:*** *Comparison of changes in the peristimulus time histograms (PSTH) of area 4's reciprocally organized neurons, in simulated area 4's reciprocally organized phasic (DVV) cell activities, in PSTH of area 4's bidirectional neurons, and in simulated area 4's co-contractive (P) cell activities for flexion (A and C) and extension (B and D) movements in an MPTP-treated monkey. The vertical bars indicate the onset of movement. Spike discharges related to successive movements are accumulated into histograms, with each bin corresponding to 10 ms. In the simulations, a GO signal of G=0.1, b=120.5, g=0.7, and dopamine DA1=0.9, DA2=0.7, DA3=0.8, DA4=0.8, DA5=0.9, DA6=0.8, DA7=0.8, DA8=0.9 (MPTP-treated) were used. Note that 1 s of time is approximately 100 time steps.*

In these studies, both normal and MPTP-treated monkeys were trained to perform fast ballistic flexion and extension movements of the forearm, while recordings were made of their primary motor cortical activities and electromyographic (EMG) responses. One notable finding was a reduction in the discharge frequency of flexion and extension reciprocal (RO) cells, particularly evident in the firing intensity of flexion cells (compare RO activities in normal and MPTP cases) (Doudet et al., 1990). These figures clearly indicate that the firing intensity of flexion cells is more profoundly affected (reduced) compared to that of extension cells.

Area 4 bidirectional neuronal activity (P) is depicted by:

$$P = \left[G\left(DA_2 V_i - DA_3 V_j\right) + \frac{B_P}{DA_4}\right]^+ \qquad (4)$$

It's noteworthy that in Eqs. (3) and (4), parameters DA2 and DA3 modulate the activities of the DV flexion and extension cells, respectively, while parameter DA4 enhances the baseline activity of the DVV (Eq. 3) and P (Eq. 4) cells. These assumptions were directly derived from experimental observations (Doudet et al., 1990; Watts & Mandir, 1992; Gross, Feger, Seal, Haramburu, & Bioulac, 1983), indicating an overall reduction in the firing intensity of primary motor cortical cells (DVV and P signals) (refer to Section 4.1 and Figs. 5 and 6) and an increase in baseline activity (refer to Fig. 7 and Section 4.1) following MPTP administration.

**Journal of Information Systems Engineering and Management**
2025, 10(42s)
e-ISSN: 2468-4376
https://www.jisem-journal.com/

**Research Article**

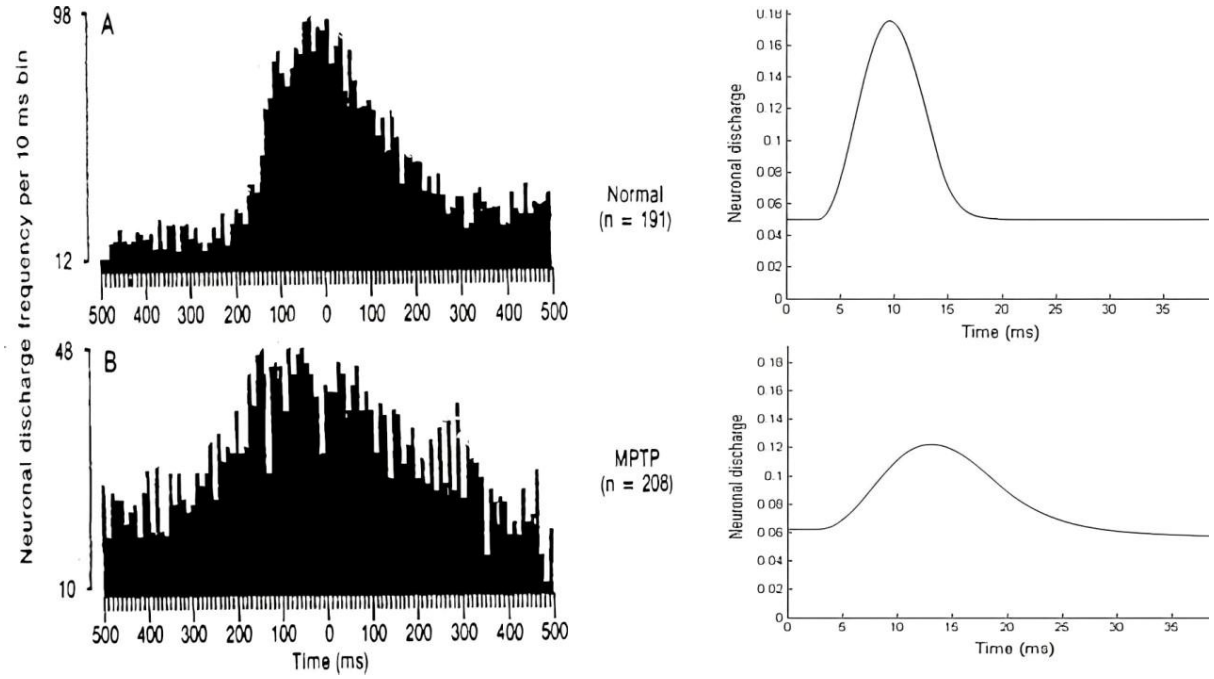


***Fig 7: (A)*** *Comparison of peristimulus histograms (PSTH) of monkey primary motor cortex task-related neuronal activity (column 1) and simulated area's 4 phasic-MT cell activity (column 2) in normal state. (B) Comparison of peristimulus histograms (PSTH) of monkey primary motor cortex task-related neuronal activity (column 1) and simulated area's 4 phasic-MT cell activity (column 2) in MPTP state. The y-axes represent the number of spikes in a time bin of 10 ms. The x-axes represent time in ms. Note, in the hemiparkinsonian (MPTP) state, an overall reduction of firing intensity, an increase in baseline activity and a reduced rate of change of neuronal discharge.*

Area 4 tonic cell activity (From, Wise, & Evarts, 1984; Kalaska et al., 1989), represented by the present position vector (PPV) dynamics, is described as follows:

$$\frac{dA_i}{dt} = G[DA_2V_i]^+ - G[DA_3V_j]^+ \quad (5)$$

The quadratic force-length relationship of muscle is approximated by:

$$F_i = k([L_i - \tau_i + C_i]^+)^2 \quad (6)$$

where k is a scaling parameter, Fi represents muscle force, Li denotes muscle length, $\tau_i$ indicates resting muscle length, Ci represents muscle contractile state, and indices i belong to {1,2} and designate antagonist muscle pairs. The dynamics of muscle contractile state are defined by:

$$\frac{dC_i}{dt} = \beta_i[(B_i - C_i)M_i - C_i] - [F_i - \Gamma_F]^+ \quad (7)$$

where GF represents the force threshold, Mi signifies the alpha-motoneuron (a-MN) pool activity in muscle control channel i, bi represents the contractile rate, and Bi denotes the number of contractile fibers recruited. The origin-to-insertion muscle lengths for opponent mono-articular muscles indicate that a change in joint angle always results in a length increment in one muscle and a reduction in length in its opponent, are defined as:

$$L_1 = \sqrt{(Cos\theta)^2 + (21 - Sin\theta)^2} \quad (8)$$

And

$$L_2 = \sqrt{(Cos\theta)^2 + (21 + Sin\theta)^2} \quad (9)$$

The dynamics of limb movement for single joint movements are defined as:

**Journal of Information Systems Engineering and Management**
2025, 10(42s)
e-ISSN: 2468-4376
https://www.jisem-journal.com/

**Research Article**

$$\frac{d^2\theta}{dt^2} = \frac{F_1 - F_2 + F_e - \eta\frac{d\theta}{dt}}{I_m} \quad (10)$$

where Fe represents an external force, Fi is the muscle force of muscle i, dQ/dt represents the angular velocity in radians, Im is the moment of inertia, and h is the joint viscosity coefficient. The contraction rate, influenced by the size principle of motor unit organization (Henneman, 1957, 1985), is defined by:

$$\beta_i = 0.05 + 0.01(A_i + P + E_i) \quad (11)$$

where Ai denotes the descending present position command, P represents the coactivation signal, and Ei signifies the stretch feedback from the spindles. Similarly, the number of contractile fibers recruited into force production also depends on the net excitatory drive to the alpha-motoneuron (a-MN):

$$B_i = 0.3 + 3(A_i + P + E_i) \quad (12)$$

The activity of Renshaw population cells is modelled by

$$\frac{dR_i}{dt} = (5B_i - R_i)DA_5 z_i M_i - R_i(0.8 + DA_6 R_j) \quad (13)$$

The recruitment rate of Renshaw cells, denoted as zi, is given by:

$$z_i = 0.05(1 + M_i) \quad (14)$$

and it is dependent on the level of activation of alpha-motoneurons (a-MN). The output signal of the Renshaw population is:

$$R_i^+ = \max(0, R_i) \quad (15)$$

which equals Ri, where Ri represents Ro. The activity of the alpha-motoneuron (a-MN) population is described by the following equation:

$$\frac{dM_i}{dt} = (\lambda B_i - M_i)DA_7\left(A_i + P + E_i + Z_j^+\right) - (M_i + 1.57)DA_8(0.19 + R_i + X_i + I_j^+) \quad (16)$$

where Xi represents the force feedback from type Ib interneurons (IbIN), and Zj is a signal dependent on the rate of change of force feedback from IbIN in the opponent muscle channel. The output signal of the a-MN population is:

$$M_i^+ = \max(0, M_i) \quad (17)$$

The population activity of type Ia interneurons (IaIN) is defined as:

$$\frac{dI_i}{dt} = (9.8 - I_i)(A_i + P + E_i) - (I_i + 1)(1 + R_i + I_j^+) \quad (18)$$

and its output signal is:

$$I_i^+ = \max(0, I_i) \quad (19)$$

The activity of IbIN population is stimulated by pathways originating from force-sensitive Golgi tendon organs. Two other activities related to Golgi tendon organ feedback are defined:

$$\frac{dX_i}{dt} = 0.1(4.5 - X_i)F_i - X_i(0.72 + 0.13X_j) \quad (20)$$

Two additional functions associated with Golgi tendon organ feedback are defined as:

$$\frac{dY_i}{dt} = 0.1(4.5 - Y_i)F_i - Y_i(0.91 + X_i) \quad (21)$$

$$\frac{dZ_i}{dt} = 0.1(4.5 - Z_i)Y_i - Z_i \quad (22)$$

This population's output signal is:

$$Z_i^+ = \max(0, Z_i - 0.1) \quad (23)$$

The static gamma-motoneuron (g-MN) activity is described by:

Journal of Information Systems Engineering and Management
2025, 10(42s)
e-ISSN: 2468-4376
https://www.jisem-journal.com/

Research Article

$$\frac{dS_i}{dt} = 4.5(1.89 - S_i)(A_i + P) - (S_i + 1.05)[0.1 + 0.23h(R_i)] \quad (24)$$

where h(w) represents the function w divided by (0.3 times w), and its output signal is:

$$S_i^+ = \max(0, S_i) \quad (25)$$

The intrafusal muscle contraction associated with static g-MN activation is described by:

$$\frac{dU_i}{dt} = (2 - U_i)S_i^+ - U_i \quad (26)$$

The activity of dynamic gamma-motoneurons (g-MNs) is given by:

$$\frac{dD_i}{dt} = (8.5 - D_i)(90G[V_i]^+ + P) - (D_i + 1.8)(1 + 90G\left[V_j\right]^+ + 0.4h(R_i)) \quad (27)$$

and its output signal is:

$$D_i^+ = \max(0, D_i) \quad (28)$$

The intrafusal muscle contraction associated with dynamic gamma-motoneuron (g-MN)activation is described as:

$$\frac{dN_i}{dt} = 0.5(1.5 - N_i)D_i^+ - 8N_i \quad (29)$$

The activation of spindle receptors was defined as:

$$\frac{dW_i}{dt} = (2 - W_i)([U_i + L_i - \Gamma_i]^+) + G_V\left(\left[N_i + \frac{dL_i}{dt}\right]\right)^+ - 8W_i \quad (30)$$

The feedback is represented by:

$$E_i = G_s W_i \quad (31)$$

where Gs denotes the feedback gain signal. It's worth noting that in Eqs. (18, 20, 24-29), dopamine (DA) is not considered. Although the effects of DA depletion on Ia (Bathien & Rondot, 1977; Obeso, Quesada, Artieda, & Martinez-Lage, 1985), Ib (Delwaide, Pepin, & Maertens de Noordhout, 1991; McCrea, 1992), and static and dynamic g-MNs activities (Hagbarth, Wallin, Lofstedt, & Aquilonius, 1975) have been extensively studied, evidence suggests that spinal Ia and Ib inhibitory interneurons play a role in Parkinson's disease (PD) rigidity (Delwaide et al., 1991; Obeso et al., 1985), while g-MNs play a role in PD tremor (Hagbarth et al., 1975; Young, 1984). Whether rigidity and tremor contribute to bradykinesia in PD remains unclear. It has been reported that rigidity, tremor, and bradykinesia occur independently (Jankovic, 1987). Therefore, we focus our paper solely on PD bradykinesia.

### System Configuration

The simulation work has been carried out using MATLAB R2019a (i5 Intel processor, 8GB RAM machine) and the differential equations were numerically integrated using MATLAB's implicit differential equation solvers, ode45, with a time step of $\Delta t$ = 0.001 ms. The relative error tolerance was set to $10^{-4}$.

## RESULTS

### The impact of dopamine depletion on the task-specific firing patterns of neurons in the primary motor cortex:

Figure 5 presents a qualitative comparison between cortical neuronal profiles (column 1 of Fig. 5A-D; based on Doudet et al. (1990)) and model cell responses (column 2 of Fig. 5A-D) in area 4 for flexion, extension, and co-contraction in normal monkeys during a simple voluntary reaching task (refer to Section 3.2 for a detailed description of the experimental study by Doudet et al. (1990)). The experimental data demonstrate a reciprocal organization of cellular activity (column 1 of Fig. 5A and B), along with the activity of bidirectional neurons tuned to both movement directions (column 1 of Fig. 5C and D). The model successfully replicates the activities of both reciprocal (represented by DVV activity) and bidirectional neurons (co-contraction signal, P) (column 2 of Fig. 5A-D).

In other research, Watts & Mandir (1992) and Gross et al. (1983) explored the impact of MPTP-induced parkinsonism on task-related neuronal activity in the primary motor cortex and motor behavior in monkeys engaged in simple

**Journal of Information Systems Engineering and Management**
2025, 10(42s)
e-ISSN: 2468-4376
https://www.jisem-journal.com/

**Research Article**

flexion and extension movements of the wrist and elbow, respectively. Watts & Mandir (1992) documented a decline in peak discharge frequency, an elevation in baseline activity, and an increase in latency between the onset of neuronal activity in the primary motor cortex (M1) and movement initiation, as well as prolonged afterdischarge duration following movement onset in the hemi-parkinsonian state. Similarly, Gross et al. (1983) observed a comparable reduction in maximal discharge frequency in lesioned animals compared to normal subjects.

Figure 6 illustrates qualitative simulations of reciprocally and bidirectionally activated neurons under conditions of reduced basal ganglia output and depleted cortical and spinal dopamine (DA1 = 0.9, DA2 = 0.7, DA3 = 0.8, DA4 = 0.8, DA5 = 0.9, DA6 = 0.8, DA7 = 0.8, DA8 = 0.9, G0 = 0.1, b = 120.5, g = 0.7; all other parameters remained the same as in the normal case). Notably, the value of parameter DA1 exceeds those of DA2, DA3, and DA4. Recall that parameter DA1 modulates the PPV input to area 5 phasic (DV) cell activity (Eq. (2)), while parameters DA2, DA3, and DA4 modulate the DV inputs to DVV and P cell activity (area 4 RO and BD activities) and DVV baseline activity (Eqs. (3) and (4)), respectively. As discussed in Section 2.1, DA afferents are denser in area 4 than in area 5, implying a stronger effect of DA depletion in area 4 compared to area 5.

Furthermore, in Figure 6, there is a noticeable overall reduction in firing intensity (Doudet et al., 1990; Gross et al., 1983), a decreased rate of change of neuronal discharge (Doudet et al., 1990; Gross et al., 1983), a disruption of neuronal activity (markedly reduced neuronal direction specificity) (Doudet et al., 1990), and an elevation in baseline activity (in the normal case, the baseline activity was 0.05, whereas in dopamine-depleted conditions, the baseline activity increased to approximately 0.07) (Doudet et al., 1990). Similar alterations in neuronal activity, including an increase in baseline activity, are evident in Figure 7 (Watts & Mandir, 1992).

Moreover, there is an elongation of neuron discharge duration in area 4 both preceding (TA, in ms; Figure 11) and following (TB, in ms; Figure 11) movement onset (OM), resulting in an extension of the total response duration, mirroring observations from experimental studies (Benazzouz, Gross, Dupont, & Bioulac, 1992; Doudet et al., 1990; Gross et al., 1983; Watts & Mandir, 1992). In our model simulations, TA was measured as the time interval between the initial deviation of cellular discharge from baseline activity to movement onset, while TB was the interval from movement onset until neuronal activity returned to baseline levels (end of cellular discharge). A schematic representation of these time intervals is illustrated in Figure 3.

Figure 8 presents a qualitative contrast between aberrant cellular reactions of GPi neurons to striatal stimulation in MPTP-treated monkeys (Figure 8A) (Tremblay, Filion, & Bedard, 1989) and simulated oscillatory GPi neuronal responses (Figure 8B). In their investigation, Tremblay et al. (1989) did not propose a functional role for such oscillatory responses. We suggest that these GPi oscillatory responses (repetitive GO signal; Figure 15A), which include at least two inhibitory-excitatory sequences (refer to the beginning of the second paragraph of the section "GPi neurons" and Figures 2 and 6 in the Tremblay et al., 1989 study), act as a gating mechanism (multiplication) for the DV signal. This process generates repetitive volitional motor commands (DVV signals; not depicted), leading to repetitive bursts of agonist-antagonist muscle activity (see Figure 10), sometimes necessary for PD patients to achieve the full amplitude of movement.

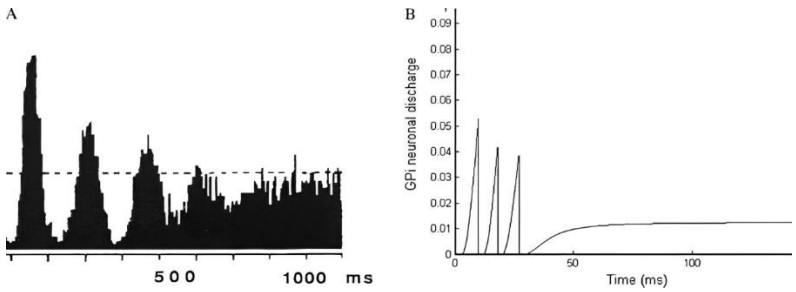


***Fig 8:*** *Comparison of (A) peristimulus histograms (PSTH) depicting abnormal oscillatory responses of GPi neurons to striatal stimulation in MPTP-treated monkeys and (B) simulated disrupted oscillatory GPi responses. Note: oscillatory responses consist of at least two inhibition–excitation sequences. The bin width is 6 ms. Parameter set: G=0.15, b=100.5, g=0.8, DA1,3,4,8=0.9, DA2,6,7=0.8, DA5=1, all other parameters remain unchanged. Time units are in milliseconds.*

**Journal of Information Systems Engineering and Management**
2025, 10(42s)
e-ISSN: 2468-4376
https://www.jisem-journal.com/

**Research Article**

## The impact of dopamine depletion on electromyography (EMG) activity

In individuals without Parkinson's disease, single ballistic movements at a joint typically exhibit a distinct biphasic pattern of electromyography (EMG) activity in both agonist and antagonist muscles. The initial agonist burst generates the force required for movement initiation, while the subsequent antagonist activity serves to decelerate the limb's motion. Occasionally, a second agonist burst is necessary to bring the limb to its intended final position. In bradykinetic patients with Parkinson's disease, the magnitude of the initial agonist burst is diminished. Although movements may still be executed relatively normally within a certain range, there are instances where additional bursts of EMG activity are required for the limb to reach its target position. The underlying cause of this inappropriate scaling of the initial agonist burst and the emergence of repetitive triphasic patterns of muscle activation in Parkinson's disease movements remains unclear.

The model outlined in this paper offers a feasible explanation for the reduction in EMG agonist burst activity observed in Parkinson's disease (PD) and why, in certain instances, multiple agonist-antagonist-agonist bursts are necessary to complete movements. We suggest that disturbances in GPi neuronal activity (the output of the basal ganglia) and dopamine depletion in the cortex, which have been shown to disrupt the reciprocal organization of M1 neurons, lead to a decrease in their activity and an increase in their rate of change. Additionally, dopamine depletion in critical cellular sites of the spinal cord results in the reduction of the size of the initial agonist burst and an increase in its rate of change. Consequently, additional EMG bursts are required for the subject to successfully execute the movement and reach the target (refer to Fig. 10).

Figure 9 illustrates a qualitative comparison between the normal (Fig. 9A) and dopamine-depleted (Fig. 9B) simulated alpha motoneuronal (aMN) activities of the agonist (row 1) and antagonist (row 2) muscles, alongside experimentally obtained muscle activations (Godaux, Koulischer, & Jacquy, 1992) during small amplitude movements. In their experimental setup, Godaux et al. (1992) assessed control and PD subjects' performance in a rapid button-pressing task while recording their EMG activities. They observed a significant reduction in peak agonist and antagonist amplitudes as well as their rate of development in Parkinson’s disease patients. Unlike some PD studies (Benazzouz et al., 1992; Doudet, Gross, Lebrun-Grandie, & Bioulac, 1985; Hayashi et al., 1988) that reported co-contraction of agonist and antagonist muscles, Godaux et al. (1992) observed a non-disrupted biphasic pattern of muscle activation (Fig. 9B). Several other human and animal studies have noted similar reductions in the rate of development and peak amplitude of the first agonist burst of EMG activity (Corcos, Chen, Quinn, McAuley, & Rothwell, 1996; Doudet et al., 1990; Hallett & Kalaska et al., 1989; Watts & Mandir, 1992). Model simulations also showed comparable reductions in the size of the agonist and antagonist bursts and their rate of change (column 2 of Fig. 9B; refer to Table 1 for the numerical value of peak agonist burst (EMGmax) in dopamine-depleted cases). A non-cocontractive agonist–antagonist pattern of muscle activation was also observed (column 2 of Fig. 9B). Additionally, dopamine depletion had a minor effect on premotor reaction time (increasing from 0.0243 in the normal case to 0.026 in the DA lesioned case; see Table 1), as observed in the study by Benazzouz et al. (1992), but significantly increased the electromechanical delay time (from 13.10 in the normal case to 17.90 in the DA-depleted case; see Table 1) (Benazzouz et al., 1992; Doudet et al., 1990; Gross et al., 1983).

**Journal of Information Systems Engineering and Management**
2025, 10(42s)
e-ISSN: 2468-4376
https://www.jisem-journal.com/

**Research Article**

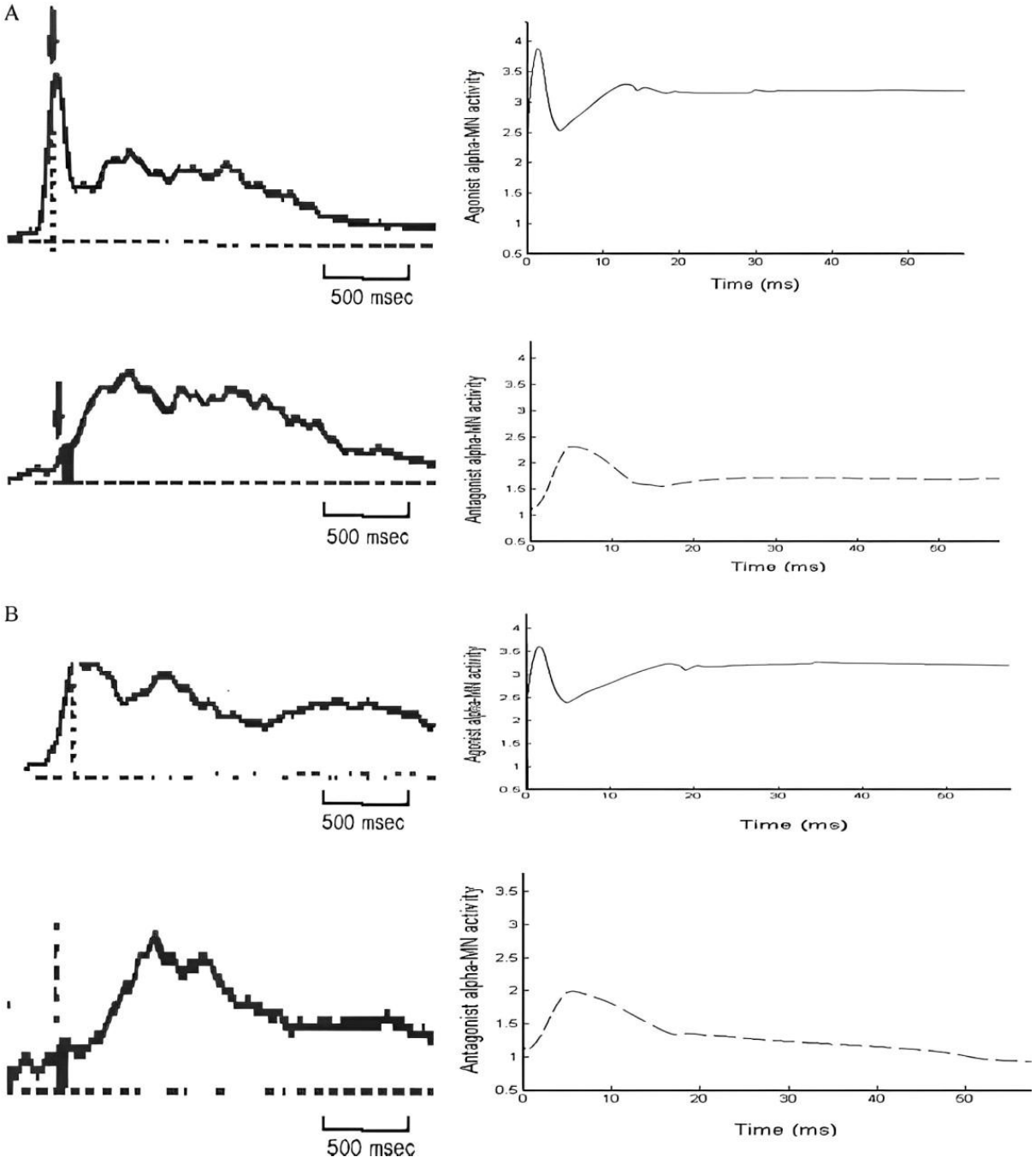


***Fig 9:*** *(A) Comparison of electromyographic (EMG) recordings and simulated alpha motoneuronal (MN) activity for an agonist muscle (row 1) and antagonist muscle (row 2) during a normal movement. The arrow indicates the onset of movement (OM). Time units are in milliseconds. (B) Comparison of electromyographic (EMG) and simulated alpha motoneuronal (MN) activity for an agonist muscle (row 1) and antagonist muscle (row 2) during a movement in Parkinson's disease (PD). The dashed line represents the onset of movement (OM). Parameter set for PD condition: G=0.2, b=100.5, g=0.8, DA1,3,4,8=0.9, DA2,6,7=0.8, DA5=0.95. Time units are in milliseconds.*

Fig. 10 illustrates the impact of disrupted basal ganglia (BG) output (Fig. 15A) and dopamine (DA) depletion in the cortex and spinal cord during large amplitude movements, where a single biphasic agonist-antagonist muscle burst pattern is inadequate to complete the movement. Instead, a repetitive biphasic pattern of muscle activation is clearly evident (highlighted by the arrows) (Hallett & Khoshbin, 1980). Fig. 15A depicts the dynamics of the depleted GO

**Journal of Information Systems Engineering and Management**
2025, 10(42s)
e-ISSN: 2468-4376
https://www.jisem-journal.com/

**Research Article**

signal responsible for generating this repetitive EMG activity. As detailed in Section 4.1, the generation of such a repetitive biphasic pattern of muscle activation results from gating the difference vector (DV) signal through multiple inhibition-excitation sequences of abnormal globus pallidus interna (GPi) activity (Fig. 8), facilitating the generation of multiple volitional motor cortical commands transmitted to the spinal cord to complete the movement.

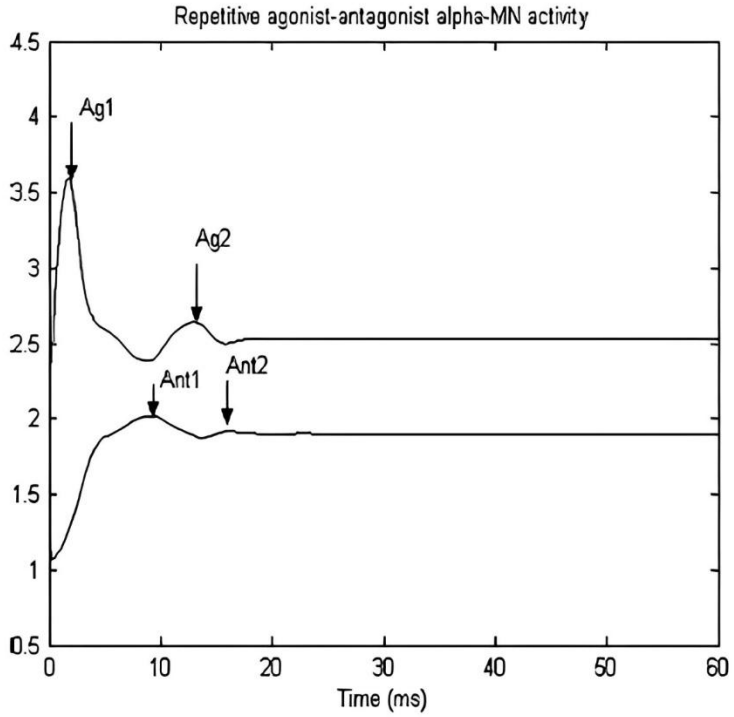


***Fig 10:*** *Recreating the repetitive biphasic alpha motoneuronal (MN) activity observed in a movement affected by dopamine depletion, this illustration showcases the essential bursts of agonist-antagonist pairs necessary for executing the motion. Each pair denotes a distinct sub-movement within the sequence. Specifically, to accomplish the entire movement, two sets of agonist-antagonist pairs are required. The first pair (Ag1 and Ant1) initiates the movement, while the subsequent pair (Ag2 followed by Ag1, and Ant2 followed by Ant1) ensures the completion of the movement's full range of motion.*

## The impact of dopamine depletion on movement variables

Figures 3 and 4 outline the variables discussed in this section. Let's define these movement variables: Cellular Reaction Time (CRT) is the duration from the simulation's start to the onset of neuronal activity change. Premotor Reaction Time (PMT) is the period from the simulation's start to the onset of EMG activity in the agonist muscle. Electromechanical Delay (EMD) is the duration between the onset of EMG activity in the agonist muscle and the movement's initiation. Reaction Time (RT) encompasses PMT and EMD. Time-to-Peak (TPV) is the duration from movement onset to peak velocity. Movement Time (MT) spans from movement onset to completion. Deceleration Time (DT) extends from peak velocity to movement end. Peak Velocity (Vmax) denotes the maximum velocity reached, and Peak EMG (EMG max) signifies the highest EMG activity level recorded.

Figure 11 illustrates a qualitative comparison between forearm angular displacement (column 1; adapted from Gross et al., 1983) and a simulated position trace (column 2), focusing on movement onset in both normal (Figure 11A) and dopamine-depleted (Figure 11B) cases. Movement onset and termination were automatically estimated using an algorithm (Teasdale, Philips, & Stelmach, 1993): (1) finding the maximum velocity value (Vmax); (2) locating the sample where the time series exceeds 10% of Vmax; (3) searching for the first sample, from this point back to the beginning of movement, where the velocity is between (0.1 Vmax) and (0.01 Vmax); this sample marks the onset. Movement end was determined using a similar reverse algorithm. In Figures 11A and B, alongside the position traces, horizontal histograms of Cellular Reaction Time (CRT), the neuronal time interval preceding movement onset (TA),

**Journal of Information Systems Engineering and Management**
2025, 10(42s)
e-ISSN: 2468-4376
https://www.jisem-journal.com/

**Research Article**

the time interval following movement onset (TB), and movement end (ME) are depicted with four vertical dashed lines. In Figure 11B, movements remain smooth, but both Reaction Time (RT) and Movement Time (MT) are significantly increased due to dopamine depletion (Benazzouz et al., 1992; Camarata et al., 1992; Doudet et al., 1990; Gross et al., 1983; Rand et al., 2000; Watts & Mandir, 1992; Weiss et al., 1996) (see Table 1 for numerical values). While CRT is only slightly affected by dopamine depletion, TA is markedly increased (Doudet et al., 1990; Gross et al., 1983).

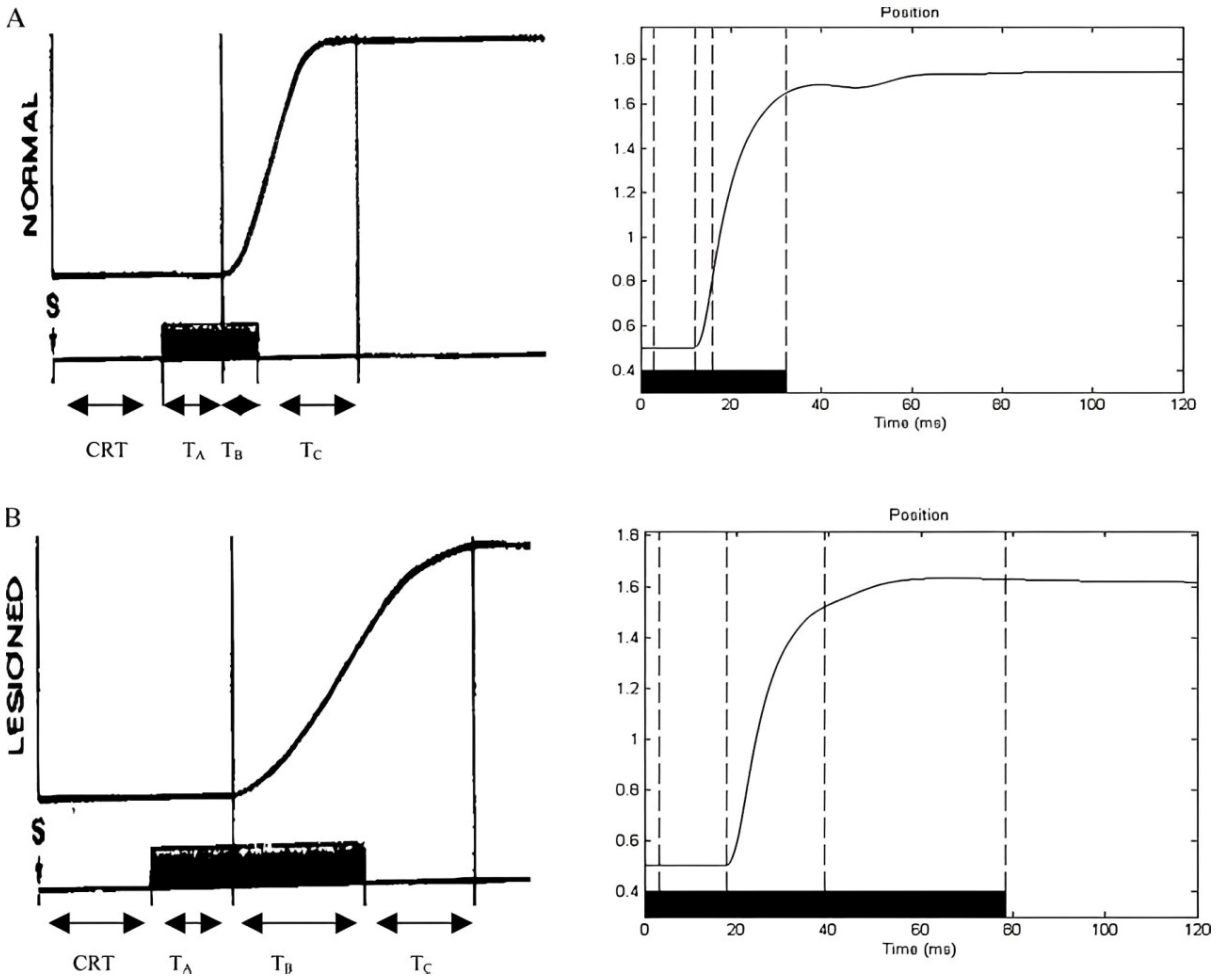


***Fig 11:*** *Comparison between simulated (column 2) and experimentally acquired forearm displacement (position) under normal (A) and Parkinson's disease (B) conditions is depicted. The shaded area illustrates the neuronal changes associated with movement. In both A and B: (column 1) the vertical bar denotes the onset of forearm displacement; S indicates the auditory cue; CRT represents the mean cellular reaction time; TA signifies changes in neuronal activity preceding the onset of movement (OM); TB denotes changes in neuronal activity following OM; TC reflects changes in neuronal activity from TB until the movement's end (ME). (column 2) The time interval between the vertical dashed lines, from left to right, represents CRT, TA, TB, and TC, respectively. The parameter set for Parkinson's disease condition is: G0=0.2, b=100.5, g=0.8, DA1,3,4,8=0.9, DA2,6,7=0.8, DA5=0.95. Time units are in milliseconds.*

Figure 12 presents a qualitative analysis comparing velocity profiles obtained experimentally (column 1; adapted from Godaux et al., 1992) with simulated velocity traces (column 2) for both normal (Fig. 12A) and PD (Fig. 12B) conditions. The insets offer a glimpse into the dynamics of the GO signals utilized. In the normal condition, the velocity profile demonstrated a single peak and smooth progression (Abend, Bizzi, & Morasso, 1982), akin to a seamless acceleration followed by deceleration (Abend et al., 1982). In contrast, the dopamine-depleted condition exhibited a diminished peak velocity, prolonged time-to-peak, and extended movement duration (Camarata et al., 1992; Watts & Mandir, 1992; Weiss et al., 1996).

**Journal of Information Systems Engineering and Management**
2025, 10(42s)
e-ISSN: 2468-4376
https://www.jisem-journal.com/

**Research Article**

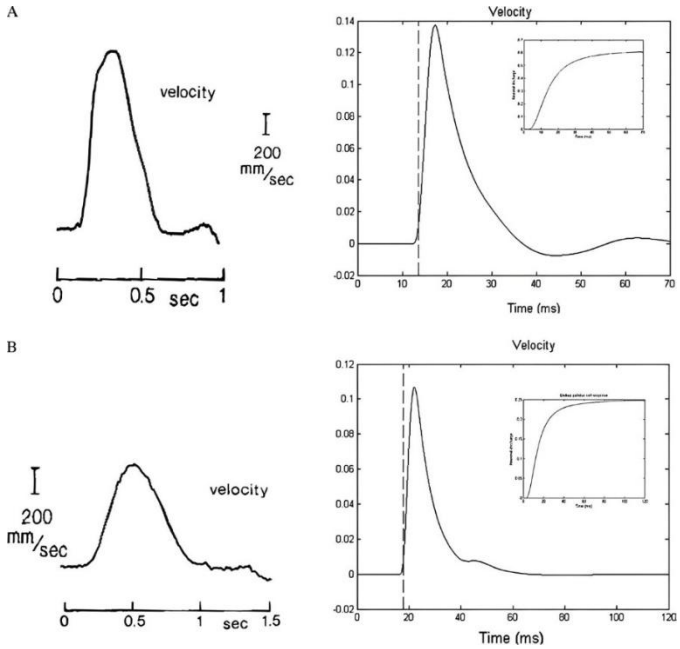


***Fig 12:*** *Comparison between simulated (column 2) and experimentally acquired (column 1; reproduced with permission from Godaux et al., 1992, Fig. 3, p. 96, Copyright Wiley-Liss, Inc., a subsidiary of John Wiley & Sons, Inc) velocity profiles in normal (A) and Parkinson's disease (B) conditions is presented. Insets depict the dynamics of the GO signal in normal (A) and PD (B) conditions. The parameter set for the PD condition is: GoZo.2, bZ100.5, gZo.8, DA1,3,4,8Zo.9, DA2,6,7Zo.8, DA5Zo.95. Time units are in milliseconds.*

Figure 13 illustrates model-simulated muscle force curves for both normal (Fig. 13A) and PD (Fig. 13B) conditions. In the normal scenario, there's a clear agonist-antagonist-agonist pattern of muscle activation (Fig. 13A). However, this pattern is disrupted in the absence of dopamine within the network. Experimental findings (Stelmach, Teasdale, Phillips, & Worringham, 1989) report a reduction in maximum peak force and an increase in time-to-peak force in such instances. In the simulations, the maximum peak force value decreased from 0.062 to 0.04. Additionally, there's a complete absence of the antagonist burst and nearly complete absence of the second agonist burst (with its peak value less than 0.001) observed (Fig. 12B; Berardelli et al., 1986).

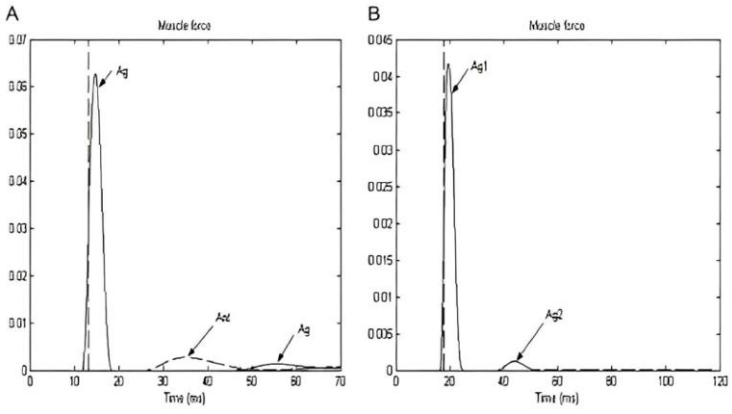


***Fig 13:*** *Contrasting simulated muscle force in normal (A) and Parkinson's disease (B) conditions is illustrated. Arrows highlight the bursts of agonist-antagonist activity. The parameter set for the Parkinson's disease condition is: Go=0.2, b=100.5, g=0.8, DA1,3,4,8=0.9, DA2,6,7=0.8, DA5=0.95. Time units are in milliseconds.*

Figure 14 displays various velocity curves corresponding to the depletion of BG and DA in the cortex and spinal cord. The data clearly indicate that reaction time (RT) lengthens with greater depletion of DA. Notably, motor impairment

**Journal of Information Systems Engineering and Management**
2025, 10(42s)
e-ISSN: 2468-4376
https://www.jisem-journal.com/

**Research Article**

becomes more pronounced at 'medium' levels of DA depletion (indicated by dotted lines). Moreover, movement time (MT) extends as DA levels decrease, evidenced by lower peak velocities and elongated velocity profiles (bradykinesia). According to the model's predictions, the severity of motor impairment correlates with the extent of DA depletion.

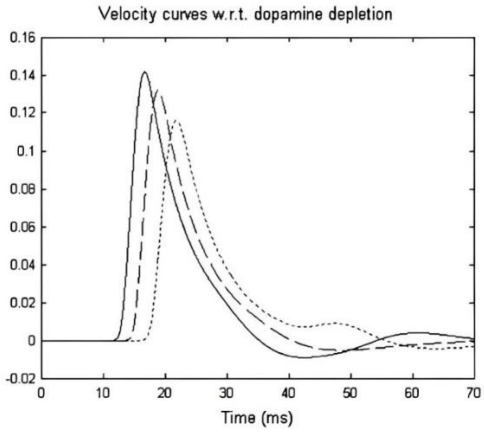


***Fig 14:*** *Simulated velocity curves are depicted as dopamine (DA) levels decrease progressively in the model. Solid lines represent normal conditions (G0=0.6, b=100.5, g=0.8, DA1–8=1); dashed lines illustrate 'low' DA depletion (G0=0.4, b=100.5, g=0.8, DA1=0.95, DA2= 0.75, DA3=0.85, DA4=0.85, DA5=0.95, DA6=0.85, DA7=0.85, DA8=0.95); and dotted lines signify 'medium' DA depletion (G0=0.2, b=100.5, g=0.8, DA1=0.9, DA2=0.7, DA3=0.8, DA4=0.8, DA5=0.9, DA6=0.8, DA7=0.8, DA8=0.9). The simulation cases of 'medium' and 'low' DA depletion describe the parameter set values utilized to generate the corresponding velocity curves. It's worth noting that as the DA levels decrease, the network output demonstrates increased reaction time and movement slowness (bradykinesia). Time units are measured in milliseconds.*

In Figure 15, the velocity (B), position (C), and muscle force (D) traces of large amplitude movements are depicted. As discussed earlier, these movements required multiple motor programs characterized by a repetitive biphasic pattern of MN activation (as shown in Fig. 10). The conclusion of each motor program and the subsequent initiation of the next are clearly delineated by inflection points on the PD position curve (Fig. 15C). Both the velocity (Fig. 15B) and muscle force (Fig. 15D) curves exhibit multiple peaks and tend to feature a prolonged deceleration phase (signifying increased deceleration time; refer to Fig. 4 for a schematic definition), contrasting with the behavior observed in the normal case.

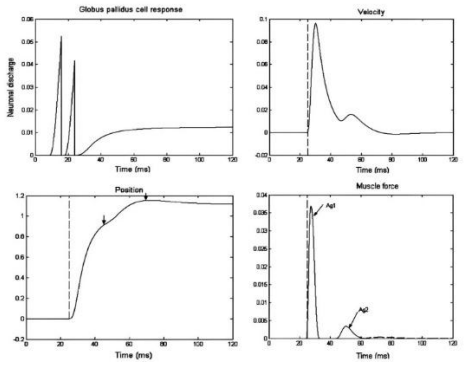


***Fig 15:*** *Simulated profiles of GO signal (A), velocity (B), position (C), and muscle force (D) are presented for a large amplitude movement in a dopamine-depleted condition. In panel A, repetitive dynamics of the GO signal are shown. Panel C highlights sub-movements (inflection points) necessary to complete the main movement, indicated by down-pointing arrows. Panel D illustrates that two agonist bursts are required to execute the movement, while antagonist bursts are absent. The vertical dashed bar denotes the onset of movement (OM). The parameter set used is: G0=0.15, b=100.5, g=0.8, DA1,3,4,8=0.9, DA2,6,7=0.8, DA5=1, with all other parameters remaining unchanged. Time units are measured in milliseconds.*

**Journal of Information Systems Engineering and Management**
2025, 10(42s)
e-ISSN: 2468-4376
https://www.jisem-journal.com/

**Research Article**

## Variability in endpoint movements

Camarata et al. (1992) conducted a study where they recorded velocity and acceleration profiles during two-joint horizontal planar movements in monkeys before and after MPTP treatment. Their findings revealed significant variability in the onset, peak velocity, and time-course of velocity profiles among the MPTP-treated monkeys (as shown in Fig. 16A). Similarly, in a study involving humans, Stelmach et al. (1989) observed variability in the force profiles of Parkinson's disease patients.

Figure 16 presents a comparison between the velocity profile of a post-MPTP monkey (Fig. 16A) and the simulated velocity curves of the dopamine-depleted model (Fig. 16B). As depicted in Fig. 16B, our model successfully replicated the variability observed in the onset, end, peak, and time-course of the velocity profile, consistent with findings from kinematics studies (Camarata et al., 1992; Rand et al., 2000; Stelmach et al., 1989). To achieve this, we allowed the cortical and spinal cord dopamine levels to vary within a range bounded by 0.3 (lesioned) and 1 (normal), using MATLAB's unifrnd() function to generate six random values for dopamine levels. Additionally, we manually adjusted the parameters of the GO signal, G0 and b, to ensure smooth velocity profiles. For each random dopamine value, the model was run, and velocity and time vectors were collected. Finally, all six velocity vectors were plotted against time in a single graph (Fig. 16B).

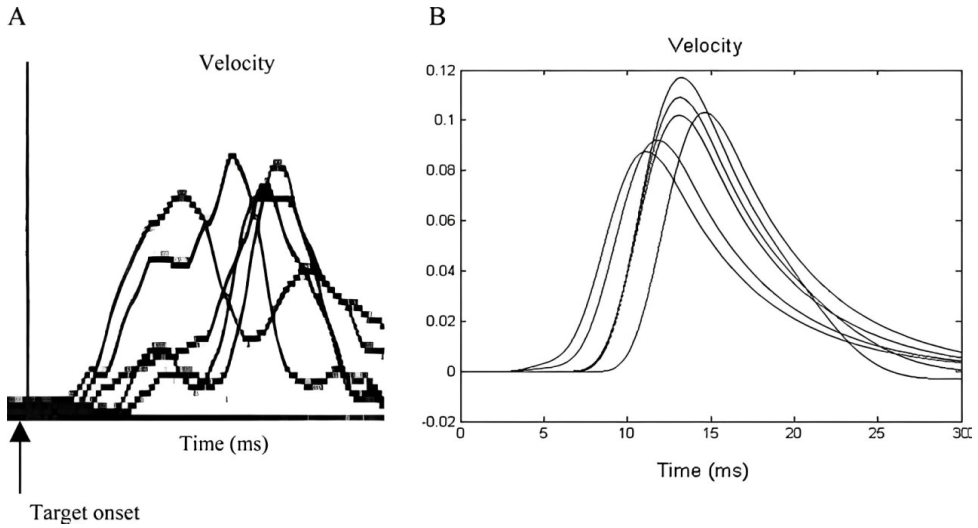


***Fig 16:*** *Contrasting velocity profiles towards a single target between post-MPTP (A) conditions and simulated dopamine-depleted (B) conditions is displayed. In panel A, profiles are synchronized with target presentation (vertical bar). It's noteworthy to observe the variability in the onset, end, peak velocity, and overall time course of the velocity profiles in both experimentally MPTP-treated and simulated dopamine-depleted conditions.*

## Which site exerts the most severe effects on neuronal activity, electromyography (EMG) signals, and movement variables?

So far, our investigation has focused on the impact of disrupted basal ganglia output and dopamine depletion in the cortex and spinal cord on various aspects such as neuronal activity in the primary motor cortex, EMG signals, and movement variables like reaction time and movement time. This leads us to the crucial question: which disrupted site has the most significant effects on these variables? To address this inquiry, we formulated three distinct cases.

- In Case 1, both cortical and spinal dopamine levels were depleted, while the output of the basal ganglia (GO signal) remained unchanged (refer to Table 2 for DA1–8 parameter values under normal, 'low', and 'medium' simulated conditions).
- In Case 2, the output of the basal ganglia was reduced (refer to Table 2 for modified b and G0 parameter values), while cortical and spinal dopamine levels were maintained normal.
- In Case 3, both the output of the basal ganglia and dopamine levels in the cortex and spinal cord were depleted (refer to Table 2 for b, G0, and DA1–8 parameter values).

Journal of Information Systems Engineering and Management
2025, 10(42s)
e-ISSN: 2468-4376
https://www.jisem-journal.com/

Research Article

**Table 2: Effects of disrupted BG output and dopamine depletion on neuronal, muscular and movement variables in three cases**

| Case 1 | Normal Basal Ganglia output | Dopamine Depletion | Cortical and Spinal Sites |
|---|---|---|---|
| F | 0.059 | 0.041 | 0.04 |
| Go | 0.6 | 0.6 | 0.6 |
| MT (ms) | 14.77 | 16.89 | 17.16 |
| DT (ms) | 11.79 | 13.53 | 13.51 |
| TPV (ms) | 2.99 | 3.36 | 3.65 |
| RT (ms) | 4.39 | 4.94 | 5.45 |
| β | 15.5 | 15.5 | 15.5 |
| Vmax | 0.11 | 0.09 | 0.09 |
| EMGmax | 1.59 | 1.4 | 1.28 |
| DVV max | 0.21 | 0.2 | 0.19 |
| DA 1,3,4,7 | 1 | 0.9 | 0.9 |
| DA 2,6,8 | 1 | 0.8 | 0.65 |
| DA 5 | 1 | 1 | 1 |
| Γ | 1 | 1 | 1 |
| **Case 2** | **Disrupted Basal Ganglia output** | **Normal Dopamine** | **Cortical and Spinal Sites** |
| F | 0.06 | 0.051 | 0.0325 |
| Go | 0.6 | 0.54 | 0.45 |
| MT (ms) | 14.77 | 16.86 | 17.75 |
| DT (ms) | 11.79 | 13.63 | 13.8 |
| TPV (ms) | 2.99 | 3.23 | 3.95 |
| RT (ms) | 4.39 | 4.55 | 4.94 |
| β | 15.5 | 16.55 | 19.4 |
| Vmax | 0.11 | 0.096 | 0.0751 |
| EMGmax | 1.59 | 1.54 | 1.43 |
| DVV max | 0.21 | 0.2 | 0.18 |
| DA 1,3,4,7 | 1 | 1 | 1 |
| DA 2,6,8 | 1 | 1 | 1 |
| DA 5 | 1 | 1 | 1 |
| Γ | 1 | 1 | 1 |

Journal of Information Systems Engineering and Management
2025, 10(42s)
e-ISSN: 2468-4376
https://www.jisem-journal.com/

Research Article

| Case 3 | Disrupted Basal Ganglia output | Dopamine Depletion | Cortical and Spinal Sites |
|---|---|---|---|
| F | 0.06 | 0.04 | 0.03 |
| Go | 0.6 | 0.54 | 0.45 |
| MT (ms) | 14.77 | 17.27 | 17.83 |
| DT (ms) | 11.79 | 13.55 | 13.41 |
| TPV (ms) | 2.99 | 3.72 | 4.42 |
| RT (ms) | 4.39 | 5.15 | 6.71 |
| β | 15.5 | 16.55 | 19.4 |
| Vmax | 0.11 | 0.08 | 0.08 |
| EMGmax | 1.59 | 1.35 | 1.15 |
| DVV max | 0.21 | 0.19 | 0.17 |
| DA 1,3,4,7 | 1 | 0.9 | 0.75 |
| DA 2,6,8 | 1 | 0.8 | 0.65 |
| DA 5 | 1 | 1 | 1 |
| Γ | 1 | 1 | 1 |

For all three cases, we examined the effects of disrupted basal ganglia output and cortical/spinal dopamine depletion on neuronal, muscular, and movement variables across three conditions: (1) normal (no disruption), (2) 'low' disruption, and (3) 'medium' disruption.

In Case 1, we observed a gradual depletion of cortical and spinal dopamine (DA) levels. The DA parameter values and results across all three simulated conditions are summarized in Table 2. The impact of cortical and spinal DA depletion is evident in several variables: peak DVV activity decreased from 0.21 at 0% depletion to 0.19 at 25%, peak EMG activity decreased from 1.59 at 0% to 1.28 at 25%, reaction time increased from 4.39 ms at 0% to 5.45 ms at 25%, movement time increased from 14.77 ms at 0% to 17.16 ms at 25%, and time-to-peak velocity increased from 2.99 ms at 0% to 3.65 ms at 25%. However, inconsistent results were observed for peak velocity (Vmax), deceleration time (DT), and muscle force (F). Specifically, Vmax decreased from 0.11 at 0% to 0.09 at 10% depletion, with no change observed at lower percentages of DA depletion. Similarly, DT increased from 11.79 at 0% to 13.53 at 10% and remained constant at 25% depletion, while F decreased to 0.04 at 10% and remained constant at that level at 25%.

In Case 2, we examined the impact of depleted basal ganglia (BG) output, characterized by a reduction in the size and rate of change of the GO signal (refer to Case 2 of Table 2 for values of b and Go parameters), on neuronal, muscular, and movement variables. The decreased size and rate of the GO signal reflect the diminished responsiveness of GPi cells observed in MPTP primates (Chevalier & Deniau, 1990; Filion, Tremblay, & Bedard, 1991; Tremblay et al., 1989). Notably, dopamine levels in the cortex and spinal cord remained unchanged (DA1–8Z1). The effects of BG dopamine depletion yielded more consistent outcomes (refer to Table 2 for values of neuronal, EMG, and movement variables). Movement time (MT), reaction time (RT), time-to-peak velocity (TPV), and deceleration time (DT) increased, while peak DVV, peak EMG, muscle force activities, and peak velocity decreased as we transitioned from the normal condition to the 'medium' disrupted condition. It's worth noting that the profile of the GO signal used in these simulations exhibited a sigmoidal shape (refer to the inset of Fig. 12B).

**Journal of Information Systems Engineering and Management**
2025, 10(42s)
e-ISSN: 2468-4376
https://www.jisem-journal.com/

**Research Article**

In Case 3, both the basal ganglia output and the dopamine levels in the cortex and spinal cord were diminished. The outcomes mirrored those observed in Case 2, but the effects were more pronounced in this instance (refer to Case 3 of Table 2 for parameter values and values of neuronal, EMG, and movement variables).

## DISCUSSION

### Common Issues

The current model serves as a representation of voluntary movement and proprioception, providing a unified interpretation of the functional roles of various cell types within movement-related regions of the primate cortex. This model is an extension and refinement of Contreras-Vidal et al.'s (1997) VITE-FLETE model, which primarily addressed psychophysical data and offered neural explanations for variables like DV, DVV, PPV, and GO. Drawing on established cortico-spinal neuroanatomical connections (refer to Tables 1 and 2 of Contreras-Vidal et al., 1997), this model's dynamic activity aligns with the neural firing patterns of key cell types found in the primary motor cortex (area 4) and parietal cortex (area 5). These cell types include reciprocal neurons, bidirectional neurons, phasic MT neurons, tonic neurons, and others, which are known to be essential for both voluntary normal movements and tasks associated with Parkinson's disease (such as bradykinesia) reaching tasks.

The model offers a comprehensive perspective on the corticospinal regulation of voluntary movement in Parkinson's disease by examining the impact of dopamine depletion on basal ganglia, cortex, and spinal cord outputs. It encompasses numerous established empirical characteristics of Parkinsonian voluntary actions, including:

- Increased cellular reaction time
- Prolonged behaviour reaction time
- Extended duration of neuronal discharge in area 4 before and after movement onset
- Reduction in firing intensity and rate of cells in the primary motor cortex
- Abnormal oscillatory response in the GPi
- Disinhibition of reciprocally tuned cells
- Elevated baseline activity
- Repetitive bursts of muscle activation
- Prolongation of premotor and electromechanical delay times
- Reduction in size and rate of development of the initial agonist burst in EMG activity
- Asymmetric increase in time-to-peak and deceleration time
- Decrease in peak velocity trace
- Increase in movement duration
- Significant reduction in size and rate of development of muscle production
- Movement variability.

These findings provide substantial evidence in support of the main hypothesis outlined earlier in the paper.

### What insights does the model provide?

The model introduces a novel prediction regarding the functional role of bidirectional neurons located in the primary motor cortex (as identified by Doudet et al., 1990). These neurons are proposed to generate a central co-contraction signal transmitted to antagonist muscles during voluntary movement. This concept was initially suggested by Humphrey & Reed (1983), who provided pioneering neurophysiological evidence indicating the existence of two distinct central systems: one responsible for the reciprocal activation of antagonist muscles and another for their coactivation. While Humphrey & Reed (1983) did not delineate the pathway through which their coactivation cells influence flexor and extensor motor neurons, other modeling endeavors (such as that by Bullock & Contreras-Vidal,

Journal of Information Systems Engineering and Management
2025, 10(42s)
e-ISSN: 2468-4376
https://www.jisem-journal.com/

Research Article

1993) envisioned the co-contractive signal as a tonic activity persisting throughout the movement. In our model, the impact of coactivation cells on flexor and extensor motor neurons is regulated by the activities of bidirectional neurons (as described in Eq. (4)), wherein the gating of the dorsal ventral input is modulated by a voluntarily adjustable GO signal to the primary motor cortex.

According to our model, we anticipated that the repetitive triphasic pattern observed in Parkinson's disease movements originates centrally. This pattern stems from the oscillatory output of basal ganglia structures, particularly the internal segment of the globus pallidus, as demonstrated by Tremblay et al. (1989). Their findings revealed oscillatory responses in MPTP-treated GPi, consisting of at least two inhibition-excitation sequences (refer to Fig. 8A). Hallett & Khoshbin (1980) illustrated that PD patients required additional triphasic muscle activation patterns to execute fast yet accurate elbow flexion movements. Each cycle of activation had a fixed duration, but the magnitudes of the bursts diminished progressively. To replicate such oscillatory behavior in our model, the tonic activation of pallidal output (i.e., the GO signal) needed to be initiated and halted multiple times within a single movement (refer to Fig. 15A). Each activation cycle of the GO signal had a fixed duration, but its magnitude decreased in successive cycles. These cycles represented motor commands sent to the lower spinal centers, ensuring the appropriate level of muscle recruitment for movement completion. However, since each activation cycle did not generate sufficient muscle activation for movement completion with a single set of agonist-antagonist bursts, additional biphasic bursts of lower intensities were necessary to finalize the movement (refer to Figs. 10 and 15B–D).

Furthermore, our model effectively replicates the variability observed in the onset, end, peak, and time-course of velocity profiles (known as movement variability) seen in Parkinson's disease kinematics studies (Camarata et al., 1992; Rand et al., 2000; Stelmach et al., 1989). In our model, we allowed the parameters of the basal ganglia output (GO signal) and dopamine levels in the cortex and spinal cord to vary randomly from trial to trial. This assumption of random variability in basal ganglia output and cortical/spinal dopamine levels seems reasonable, given that it has been long acknowledged that the predominant firing mode of dopaminergic neurons in rats is random firing (Bunney et al., 1973; Grace & Bunney, 1984a,b; Tepper, Martin, & Anderson, 1995). Moreover, damage to the nigrostriatal pathway in Parkinson's disease results in a significant reduction in dopamine content in the substantia nigra pars compacta (with more than 90% of dopamine neurons dying), leading to compensatory changes in the firing patterns of remaining dopamine neurons (Burns et al., 1983; Bezard & Gross, 1998; Grace, 1995). For instance, when dopamine neuron firing rates are low, they may fail to adequately facilitate motor cortical commands sent to the lower spinal centers, resulting in the subject's arm potentially undershooting the target. In subsequent trials, increased dopamine neuron firing rates may compensate for the subject's behavioral dysfunction, leading to either reaching the target or overshooting it due to over-facilitated motor cortical commands. This concept serves as a thought experiment warranting further investigation by neurophysiologists.

Ultimately, our model offers a thorough examination of which site exhibits the most pronounced impact on neuronal, EMG, and movement variables when dopamine levels are reduced. Our analysis indicates that while disrupted basal ganglia output exerts the most significant effect on movement, dopamine depletion in the cortex and spinal cord is necessary to enhance and validate these findings. This assumption appears reasonable, given that dopamine levels in the cortex are only 5–10%, whereas they constitute 90–95% in the basal ganglia (Tzschentke, 2001).

## LIMITATIONS AND FUTURE WORK

While our model effectively replicates many aspects of Parkinson's disease (PD) bradykinesia, it does possess several limitations. Firstly, it does not incorporate the learning process of movements, assuming that movements are already learned and stored in motor areas. Secondly, it lacks a detailed depiction of the circuitry within the basal ganglia structures. In our model, the influence of basal ganglia structures is represented by the GO signal, which is multiplied with the activity of cells in area 4 to generate a volitional command sent to spinal centers for movement generation. Thirdly, it does not address the effects of dopamine depletion on the long latency stretch response. Evidence suggests that the gain of long latency stretch responses is abnormally high in PD patients (Rothwell, Obeso, Traub, & Marsden, 1983). These responses, elicited by muscle stretch, occur later than the segmental stretch reflex, and the circuitry underlying them is subject to debate. Some researchers propose that afferent signals reach the cortex to activate corticospinal neurons, while others believe that reflexes are spinal, with the long-latency aspect attributable to

delayed afferent input. Fourthly, although our model includes spinal inhibitory interneurons, it does not consider the effects of dopamine depletion on their activities. Delwaide and colleagues (1991) suggested that the rigidity observed in PD patients results from increased excitability of motor neurons due to reduced activity of spinal inhibitory interneurons.

## REFERENCES

[1] Abbs, J. H., Hartman, D. E., & Vishwanat, B. (1987). Orofacial motor control impairment in Parkinson's disease. Neurology, 37, 394–398.
[2] Abend, W., Bizzi, E., & Morasso, P. (1982). Human arm trajectory formation. Brain, 105(Pt. 2), 331–348.
[3] Albin, R. L., Young, A. B., & Penney, J. B. (1989). The functional anatomy of basal ganglia disorders. Trends in Neurosciences, 12, 366–375.
[4] Bathien, N., & Rondot, P. (1977). Reciprocal continuous inhibition in rigidity in parkinsonism. Journal of Neurology, Neurosurgery, and Psychiatry, 40, 20–24.
[5] Benazzouz, A., Gross, C., Dupont, J., & Bioulac, B. (1992). MPTP induced hemiparkinsonism in monkeys: Behavioral, mechanographic, electromyographic and immunohistochemical studies. Experimental Brain Research, 90, 116–120.
[6] Benecke, R., Rothwell, J. C., & Dick, J. P. R. (1986). Performance of simultaneous movements in patients with Parkinson's disease. Brain, 109, 739–757.
[7] Berardelli, A., Dick, J. P. R., Rothwell, J. C., Day, B. L., & Marsden, C. D. (1986). Scaling of the size of the first agonist EMG burst during rapid wrist movements in patients with Parkinson's disease. Journal of Neurology, Neurosurgery, and Psychiatry, 49, 1273–1279.
[8] Berger, B., Trottier, S., Verney, C., Gaspar, P., & Alvarez, C. (1988a). Regional and laminar distribution of dopamine and serotonin innervation in the macaque cerebral cortex: A radioautographic study. The Journal of Comparative Neurology, 273, 99–119.
[9] Berns, G., & Sejnowski, T. (1998b). A computational model of how the basal ganglia produce sequences. Journal of Cognitive Neuroscience, 10, 108–121.
[10] Bezard, E., & Gross, C. E. (1998c). Compensatory mechanisms in experimental and human parkinsonism: Towards a dynamic approach. Progress in Neurobiology, 55, 93–116.
[11] Bjorklund, A., & Lindvall, O. (1984). Dopamine containing systems in the CNS. In A. Bjorklund, & T. Hokfelt (Vol. Eds), Handbook of chemical neuroanatomy. Classical transmitters in the CNS, Part 1 (Vol. 2) (pp. 55– 121). Amsterdam: Elsevier.
[12] Bjorklund, A., & Skagerberg, G. (1979). Evidence of a major spinal cord projection from the diencephalic A11 dopamine cell group in the rat using transmitter-specific fluoroscent retrograde tracing. Brain Research, 177, 170–175.
[13] Blessing, W. W., & Chalmers, J. P. (1979). Direct projection of catecholamine (presumably dopamine)-containing neurons from the hypothalamus to spinal cord. Neuroscience Letters, 11, 35–40.
[14] Brown, S. H., & Cooke, J. D. (1984). Initial agonist burst duration depends on movement amplitude. Experimental Brain Research, 55, 523–527.
[15] Brown, S. H., & Cooke, J. D. (1990a). Movement related phasic muscle activation I. Relations with temporal profile of movement. Journal of Neurophysiology, 63(3), 455–464.
[16] Brown, S. H., & Cooke, J. D. (1990b). Movement related phasic muscle activation II. Generation and functional role of the triphasic pattern. Journal of Neurophysiology, 63(3), 465–472.
[17] Brown, J. W., Bullock, D., & Grossberg, S. (2004). How laminar frontal cortex and basal ganglia circuits interact to control planned and reactive saccades. Neural Networks, 17, 471–510.
[18] Bullock, D., Cisek, P., & Grossberg, S. (1998). Cortical networks for control of voluntary arm movements under variable force conditions. Cerebral Cortex, 8, 48–62.
[19] Bullock, D., & Contreras-Vidal, J. L. (1993). How spinal neural networks reduce discrepancies between motor intention and motor realization. In K. Newel, & D. Corcos (Eds.), Variability and motor control (pp. 183–221). Champaign, IL: Human Kinetics Press.
[20] Bullock, D., & Grossberg, S. (1988). Neural dynamics of planned arm movements: Emergent invariants and speed-accuracy properties during trajectory formation. Psychological Review, 95, 49–90.

[21] Bullock, D., & Grossberg, S. (1989). VITE and FLETE: Neural modules for trajectory formation and tension control. In W. Hershberger (Ed.), Volitional action (pp. 253–297). Amsterdam, The Netherlands: North-Holland.
[22] Bullock, D., & Grossberg, S. (1991). Adaptive neural networks for control of movement trajectories invariant under speed and force rescaling. Human Movement Science, 10, 3–53.
[23] Bullock, D., & Grossberg, S. (1992). Emergence of triphasic muscle activation from the nonlinear interactions of central and spinal neural networks circuits. Human Movement Science, 11, 157–167.
[24] Bunney, B. S., Walters, J. R., Roth, R. H., & Aghajanian, G. K. (1973). Dopaminergic neurons: Effect of antipsychotic drugs and amphetamine on single cell activity. The Journal of Pharmacology and Experimental Therapeutics, 185, 560–571.
[25] Burns, R. S., Chiueh, C. C., Markey, S. P., Ebert, M. N., Jacobowitz, D. M., & Kopin, I. J. (1983). A primate model of parkinsonism: Selective destruction of dopaminergic neurons in the pars compacta of the substantia nigra by N-methyl-4-phenyl-1,2,3,6-tetrahydropyridine. Proceedings of the National Academy of Sciences USA, 80, 4546–4550.
[26] Camarata, P. J., Parker, R. G., Park, S. K., Haines, S. J., Turner, D. A., Chae, H., et al. (1992). Effects of MPTP induced hemiparkinsonism on the kinematics of a two-dimensional, multi-joint arm movement in the rhesus monkey. Neuroscience, 48(3), 607–619.
[27] Chapman, C. D., Spidalieri, G., & Lamarre, Y. (1984). Discharge properties of area 5 neurons during arm movements triggered by sensory stimuli in the monkey. Brain Research, 309, 63–77.
[28] Chevalier, G., & Deniau, M. J. (1990). Disinhibition as a basic process in the expression of striatal functions. Trends in Neuroscience, 13(7), 277–280.
[29] Commissiong, J. W., Gentleman, S., & Neff, N. H. (1979). Spinal cord dopaminergic neurons: Evidence for an uncrossed nigrostriatal pathway. Neuropharmacology, 18, 565–568.
[30] Connor, N. P., & Abbs, J. H. (1991). Task-dependent variations in parkinsonian motor impairments. Brain, 114, 321–332.
[31] Contreras-Vidal, J. L. (1999). The gating functions of the basal ganglia in movement control. In J. A. Reggia, E. Ruppin, & D. Glanzman (Vol. Eds.), Progress in brain research (Vol. 121).
[32] Contreras-Vidal, J. L., Grossberg, S., & Bullock, D. (1997). A neural model of cerebellar learning for arm movement control: Cortico-spino-cerebellar dynamics. Learning and Memory, 3(6), 475–502.
[33] Contreras-Vidal, J. L., & Stelmach, G. (1995). A neural model of basal gangliathalamocortical
[34] relations in normal and parkinsonian movement. Biological Cybernetics, 73, 467–476.
[35] Corcos, D. M., Chen, C. M., Quinn, N. P., McAuley, J., & Rothwell, J. C. (1996). Strength in Parkinson's disease: Relationship to rate of force generation and clinical status. Annals of Neurology, 39(1), 79–88.
[36] Delwaide, P. J., Pepin, J. L., & Maertens de Noordhout, A. (1991). Shortlatency autogenic inhibition in patients with parkinsonian rigidity. Annals of Neurology, 30, 83–89.
[37] Dormand, J. R., & Prince, P. J. (1980). A family of embedded Runge-Kutta formulae. Journal of Computational and Applied Mathematics, 6, 19–26.
[38] Doudet, D. J., Gross, C., Arluison, M., & Bioulac, B. (1990). Modifications of precentral cortex discharge and EMG activity in monkeys with MPTP induced lesions of DA nigral lesions. Experimental Brain Research, 80, 177–188.
[39] Doudet, D. J., Gross, C., Lebrun-Grandie, P., & Bioulac, B. (1985). MPTP primate model of Parkinson's disease: A mechanographic and electromyographic study. Brain Research, 335, 194–199.
[40] Dubois, A., Savasta, M., Curet, O., & Scatton, B. (1986). Autoradiographic distribution of the D1 agonist [3H]SKF 38393, in the rat brain and spinal cord. Comparison with the distribution of D2 dopamine receptors. Neuroscience, 19, 125–137.
[41] Elsworth, J. D., Deutch, A. Y., Redmond, D. E., Sladek, J. R., & Roth, R. H. (1990). MPTP reduces dopamine and norepinephrine concentrations in the supplementary motor area and cingulate cortex of the primate. Neuroscience Letters, 114, 316–322.
[42] Filion, M., Tremblay, L., & Bedard, P. J. (1991). Effects of dopamine agonists on the spontaneous activity of globus pallidus neurons in monkeys with MPTP-induced parkinsonism. Brain Research, 547(1), 152–161.

[43] Flowers, K. A. (1976). Visual 'closed-loop' and 'open-loop' characteristics of voluntary movement in patients with Parkinsonism and intention tremor. Brain, 99(2), 269–310.
[44] Fromm, C., Wise, S. P., & Evarts, E. V. (1984). Sensory response properties of pyramidal tract neurons in the precentral motor cortex and postcentral gyrus of the rhesus monkey. Experimental Brain Research, 54, 177–185.
[45] Gaspar, P., Duyckaerts, C., Alvarez, C., Javoy-Agid, F., & Berger, B. (1991). Alterations of dopaminergic and noradrenergic innervations in motor cortex in Parkinson's disease. Annals of Neurology, 30, 365–374.
[46] Gaspar, P., Stepniewska, I., & Kaas, J. H. (1992). Topography and collateralization of the dopaminergic projections to motor and lateral prefrontal cortex in owl monkeys. The Journal of Comparative Neurology, 325, 1–21.
[47] Georgopoulos, A. P., Kalaska, J. F., Caminiti, R., & Massey, J. T. (1982). On the relations between the direction of two dimensional arm movements and cell discharge in primate motor cortex. The Journal of Neuroscience, 2, 1527–1537.
[48] Ghez, C., & Gordon, J. (1987a). Trajectory control in targeted force impulses. I. Role in opposing muscles. Experimental Brain Research, 67, 225–240.
[49] Ghez, C., & Gordon, J. (1987b). Trajectory control in targeted force impulses. II. Pulse height control. Experimental Brain Research, 67, 241–252.
[50] Ghez, C., & Gordon, J. (1987c). Trajectory control in targeted force impulses. III. Compensatory adjustments for initial errors. Experimental Brain Research, 67, 253–269.
[51] Gibberd, F. B. (1986). The management of Parkinson's disease. The Practitioner, 230, 139–146.
[52] Godaux, E., Koulischer, D., & Jacquy, J. (1992). Parkinsonian bradykinesia is due to depression in the rate of rise of muscle activity. Annals of Neurology, 31(1), 93–100.
[53] Gottlieb, G. L., Latash, M. L., Corcos, D. M., Liubinskas, A. J., & Agarwal, G. C. (1992). Organizing principle for single joint movements: I. Agonist– antagonist interactions. Journal of Neurophysiology, 13(6), 1417–1427.
[54] Grace, A. A. (1995). The tonic/phasic model of dopamine system regulation: Its relevance for understanding how stimulant abuse can alter basal ganglia function. Drug and Alcohol Dependence, 37, 111–129.
[55] Grace, A. A., & Bunney, B. S. (1984a). The control of firing pattern in nigral dopamine neurons: Burst firing. The Journal of Neuroscience, 4, 2877–2890.
[56] Grace, A. A., & Bunney, B. S. (1984b). The control of firing pattern in nigral dopamine neurons: Single spike firing. The Journal of Neuroscience, 4, 2866–2876.
[57] Gross, C., Feger, J., Seal, J., Haramburu, P., & Bioulac, B. (1983). Neuronal activity of area 4 and movement parameters recorded in trained monkeys after unilateral lesion of the substantia nigra. Experimental Brain Research, 7, 181–193.
[58] Gurney, K., Prescott, T. J., & Redgrave, P. (2001a). A computational model of action selection in the basal ganglia. I. A new functional anatomy. Biological Cybernetics, 84, 401–410.
[59] Gurney, K., Prescott, T. J., & Redgrave, P. (2001b). A computational model of action selection in the basal ganglia. II. Analysis and simulation of behavior. Biological Cybernetics, 84, 411–423.
[60] Hagbarth, K. E., Hagglund, J. V., Wallin, E. U., & Young, R. R. (1981). Grouped spindle and electromyographic responses to abrupt wrist extension movements in man. Journal of Physiology (London), 312, 81–96.
[61] Hagbarth, K. E., Wallin, G., Lofstedt, L., & Aquilonius, S. M. (1975). Muscle spindle activity in alternating tremor of Parkinsonism and in clonus. Journal of Neurology, Neurosurgery, and Psychiatry, 38(7), 636–641.
[62] Hallett, M., & Khoshbin, S. (1980). A physiological mechanism of bradykinesia. Brain, 103, 301–314.
[63] Hallett, M., & Marsden, C. D. (1979). Ballistic flexion movements of the human thumb. The Journal of Physiology, 294, 33–50.
[64] Hayashi, A., Kagamihara, Y., Nakajima, Y., Narabayashi, H., Okuma, Y., & Tanaka, R. (1988). Disorder in reciprocal innervation upon initiation of voluntary movement in patients with Parkinson's disease. Experimental Brain Research, 70, 437–440.
[65] Henneman, E. (1957). Relation between size of neurons and their susceptibility to discharge. Science, 126, 1345–1347.
[66] Henneman, E. (1985). The size principle: A deterministic output emerges from a set of probabilistic connections. The Journal of Experimental Biology, 115, 105–112.

[67] Horak, F. B., & Anderson, M. E. (1984). Influence of globus pallidus on arm movements in monkeys. I. Effects of kainic acid-induced lesions. Journal of Neurophysiology, 52, 290–304.
[68] Humphrey, D. R., & Reed, D. J. (1983). Separate cortical systems for control of joint movement and joint stiffness: Reciprocal activation and coactivation of antagonist muscles. In J. E. Desmedt (Ed.), Motor control mechanisms in health and disease. New York: Raven Press.
[69] Jankovic, J. (1987). Pathophysiology and clinical assessment of motor symptoms in Parkinson's disease. In W. C. Koller (Ed.), Handbook of Parkinson's disease.
[70] Kalaska, J. F., Cohen, D. A. D., Hyde, M. L., & Prud'Homme, M. J. (1989). A comparison of movement direction-related versus load direction-related activity in primate motor cortex, using a two-dimensional reaching task. The Journal of Neuroscience, 9, 2080–2102.
[71] Kalaska, J. F., Cohen, D. A. D., Prud'Homme, M. J., & Hyde, M. L. (1990). Parietal area 5 neuronal activity encodes movement kinematics, not movement dynamics. Experimental Brain Research, 80, 351–364.
[72] Lazarus, J. C., & Stelmach, G. E. (1992). Inter-limb coordination in Parkinson's disease. Movement Disorders, 7, 159–170.
[73] Lewis, D. A., Morrison, J. H., & Goldstein, M. (1988). Brainstem dopaminergic neuronsprojecttomonkeyparietalcortex.NeuroscienceLetters,86,11–16.
[74] Lidow, M. S., Goldman-Rakic, P. S., Gallager, D. W., Geschwind, D. H., & Rakic, P. (1989). Distribution of major neurotransmitter receptors in the motor and somatosensory cortex of the rhesus monkey. Neuroscience, 32(3), 609–627.
[75] Mathews, P. B. C. (1972). Mammalian muscle receptors and their central actions. Baltimore, MD: Williams and Wilkins.
[76] McCrea, D. A. (1992). Can sense be made of spinal interneurons circuits? The Behavioral and Brain Sciences, 15, 635–829.
[77] Obeso, J. A., Quesada, P., Artieda, J., & Martinez-Lage, J. M. (1985). Reciprocal inhibition in rigidity and dystonia. In P. J. Delwaide, & A. Agnoli (Eds.), Clinical neurophysiology in Parkinsonism. Amsterdam, The Netherlands: Elsevier Science Publishers BV.
[78] Rand, M. K., Stelmach, G. E., & Bloedel, J. R. (2000). Movement accuracy constraints in Parkinson's disease patients. Neuropsychologia, 38, 203–212.
[79] Rothwell, J. C., Obeso, J. A., Traub, M. M., & Marsden, C. D. (1983). The behavior long-latency stretch reflex in patients with Parkinson's disease. Journal of Neurology, Neurosurgery, and Psychiatry, 46, 35–44.
[80] Scatton, B., Javoy-Agid, F., Rouquier, L., Dubois, B., & Agid, Y. (1983). Reduction of cortical dopamine, noradrenaline, serotonin and their metabolites in Parkinson's disease. Brain Research, 275, 321–328.
[81] Shirouzou, M., Anraku, T., Iwashita, Y., & Yoshida, M. (1990). A new dopaminergic terminal plexus in the ventral horn of the rat spinal cord. Immunohistochemical studies at the light and the electron microscopic levels. Experientia, 46, 201–204.
[82] Stelmach, G. E., Teasdale, N., Phillips, J., & Worringham, C. J. (1989). Force production characteristics in Parkinson's disease. Experimental Brain Research, 76, 165–172.
[83] Takada, M., Li, Z. K., & Hattori, T. (1988). Single thalamic dopaminergic neurons project to both neocortex and spinal cord. Brain Research, 455, 346–352.
[84] Taylor, J. G., & Taylor, N. R. (2000). Analysis of recurrent cortico-basal ganglia-thalamic loops for working memory. Biological Cybernetics, 82, 415–432.
[85] Teasdale, N., Philips, J., & Stelmach, G. E. (1993). Determining movement onsets from temporal series. Journal of Motor Behavior, 25, 97–106.
[86] Tepper, J. M., Martin, L. P., & Anderson, D. R. (1995). GABAA receptor mediated inhibition of rat substantia nigra dopaminergic neurons by pars reticulata projection neurons. The Journal of Neuroscience, 15, 3092–3103.
[87] Tremblay, L., Filion, M., & Bedard, P. J. (1989). Responses of pallidal neurons to striatal stimulation in monkeys with MPTP-induced parkinsonism. Brain Research, 498(1), 17–33.
[88] Tzschentke, T. M. (2001). Pharmacology and behavioral pharmacology of thmesocortical dopamine system. Progress in Neurobiology, 63, 241–320.
[89] Watts, R. L., & Mandir, A. S. (1992). The role of motor cortex in the pathophysiology of voluntary movement deficits associated with parkinsonism. Neurologic Clinics, 10(2), 451–469.

**Journal of Information Systems Engineering and Management**
2025, 10(42s)
e-ISSN: 2468-4376
https://www.jisem-journal.com/

**Research Article**

[90] Weil-Fugazza, J., & Godefroy, F. (1993). Dorsal and ventral dopaminergic innervation of the spinal cord: Functional implications. Brain Research Bulletin, 30, 319–324.
[91] Weiner, W. J., & Singer, C. (1989). Parkinson's disease and nonpharmacologic treatment programs. Journal of the American Geriatrics Society, 37, 359–363.
[92] Weiss, P., Stelmach, G. E., Adler, C. H., &Waterman, C. (1996). Parkinsonian arm movements as altered by task difficulty. Parkinsonism and Related Disorders, 2(4), 215–223.
[93] Wierzbicka, M. M., Wiegner, A. W., & Shahani, B. T. (1986). Role of agonis and antagonist muscles in fast arm movements in man. Experimental Brain Research, 63, 331–340.
[94] Williams, S. M., & Goldman-Rakic, P. S. (1995). Characterization of the dopaminergic innervation of the primate frontal cortex using a dopaminespecific antibody. Cerebral Cortex, 3, 199–222.
[95] Williams, S. M., & Goldman-Rakic, P. S. (1998). Widespread origin of the primate mesofrontal dopamine system. Cerebral Cortex, 8, 321–345.
[96] Young, R. R. (1984). Tremor in relation to certain other movement disorders. In L. J. Findley, & R. Capildeo (Eds.), Tremor (pp. 463–472). London, England: Macmillian Publishers Ltd.